The Influence of a Weakening of the Atlantic Meridional Overturning Circulation on ENSO

Axel Timmermann, Y. Okumura, Soon-Il An, Amy Clement, B. Dong, Éric Guilyardi, A. Hu, J. H. Jungclaus, M. Renold, Thomas F. Stocker, et al.

The Influence of a Weakening of the Atlantic Meridional Overturning Circulation on ENSO

A. TIMMERMANN,* Y. OKUMURA,* S.-I. AN,+ A. CLEMENT,# B. DONG,@ E. GUILYARDI,& A. HU,** J. H. JUNGCLAUS,++ M. RENOLD,## T. F. STOCKER,## R. J. STOUFFER,@@ R. SUTTON,@ S.-P. XIE,* AND J. YIN@@

*IPRC, SOEST, University of Hawaii at Manoa, Honolulu, Hawaii
+ Department of Atmospheric Sciences, Yonsei University, Seoul, South Korea
# RSMAS/MPO, University of Miami, Miami, Florida
@ Department of Meteorology, University of Reading, Reading, United Kingdom
& Department of Meteorology, University of Reading, Reading, United Kingdom, and IPSL/LOCEAN, Paris, France
** National Center for Atmospheric Research, Boulder, Colorado
++ Max Planck Institute of Meteorology, Hamburg, Germany
Climate and Environmental Physics, Physics Institute, University of Bern, Bern, Switzerland
@@ NOAA/Geophysical Fluid Dynamics Laboratory, and Program in Atmospheric and Oceanic Sciences, Princeton University, Princeton, New Jersey

(Manuscript received 6 September 2006, in final form 13 February 2007)

ABSTRACT

The influences of a substantial weakening of the Atlantic meridional overturning circulation (AMOC) on the tropical Pacific climate mean state, the annual cycle, and ENSO variability are studied using five different coupled general circulation models (CGCMs). In the CGCMs, a substantial weakening of the AMOC is induced by adding freshwater flux forcing in the northern North Atlantic. In response, the well-known surface temperature dipole in the low-latitude Atlantic is established, which reorganizes the large-scale tropical atmospheric circulation by increasing the northeasterly trade winds. This leads to a southward shift of the intertropical convergence zone (ITCZ) in the tropical Atlantic and also the eastern tropical Pacific. Because of evaporative fluxes, mixing, and changes in Ekman divergence, a meridional temperature anomaly is generated in the northeastern tropical Pacific, which leads to the development of a meridionally symmetric thermal background state. In four out of five CGCMs this leads to a substantial weakening of the annual cycle in the eastern equatorial Pacific and a subsequent intensification of ENSO variability due to nonlinear interactions. In one of the CGCM simulations, an ENSO intensification occurs as a result of a zonal mean thermocline shoaling.

Analysis suggests that the atmospheric circulation changes forced by tropical Atlantic SSTs can easily influence the large-scale atmospheric circulation and hence tropical eastern Pacific climate. Furthermore, it is concluded that the existence of the present-day tropical Pacific cold tongue complex and the annual cycle in the eastern equatorial Pacific are partly controlled by the strength of the AMOC. The results may have important implications for the interpretation of global multidecadal variability and paleo-proxy data.

1. Introduction

Using coupled general circulation models (CGCMs), it has been shown (e.g., Manabe and Stouffer 1988; Delworth et al. 1993; Timmermann et al. 1998; Vellinga et al. 2002; Knutti et al. 2004; Timmermann et al. 2005a,b; Dahl et al. 2005; Zhang and Delworth 2005; Broccoli et al. 2006) that a weakening or a collapse of the Atlantic meridional overturning circulation (AMOC) generates substantial cooling in the North Atlantic, while leading to slightly warmer conditions in the South Atlantic. In turn an asymmetric meridional temperature seesaw is established, which encompasses not only the tropical regions but also southern polar latitudes (Blunier et al. 1998; Stocker and Johnsen 2003) and the northern North Pacific. The tropical atmospheric response to this large-scale asymmetric meridional dipole

Corresponding author address: A. Timmermann, IPRC, SOEST, University of Hawaii at Manoa, 2525 Correa Rd., Honolulu, HI 96822.
E-mail: axel@hawaii.edu

DOI: 10.1175/JCLI4283.1

is associated with an intensification of the northeasterly trade winds, pushing the Atlantic intertropical convergence zone (ITCZ) southward, as documented by paleo-proxy data (Peterson et al. 2000) and climate model simulations (Dong and Sutton 2002; Dahl et al. 2005; Zhang and Delworth 2005). This response helps to compensate for the heat loss in the North Atlantic (Broccoli et al. 2006). The ITCZ shift is brought about by anomalous temperature advection generated by anomalous northerly winds and by increased evaporation and latent cooling. The associated northern tropical Atlantic cooling in turn feeds back to the atmospheric circulation via boundary layer responses and the linear baroclinic response described in Gill (1980). This wind response feedback helps to amplify the cooling (warming) north (south) of the equator.

A large cooling in the northern tropical Atlantic (and in particular in the Caribbean) induces a large-scale anticyclonic circulation pattern (Xie et al. 2007), which is accompanied by a northerly trade wind intensification in the northeastern tropical Pacific. This trade wind response leads to a southward displacement of the Pacific ITCZ (Zhang and Delworth 2005) and the generation of a meridional SST anomaly (Dahl et al. 2005) due to anomalous heat transports and the wind–evaporation SST (WES) feedback. These results highlight the importance of the atmospheric circulation to synchronize tropical Atlantic and Pacific climate anomalies on long time scales.

Another mechanism that was recently proposed (Hsieh and Bryan 1996; Huang et al. 2000; Goodman 2001; Cessi et al. 2004; Johnson and Marshall 2004; Timmermann et al. 2005a) to explain the synchronization between Atlantic and Pacific climate anomalies during a shutdown of the AMOC involves oceanic wave dynamics. Density anomalies in the northern North Atlantic trigger oceanic Kelvin waves that propagate southward along the American coast and subsequently along the equator. At the West African coast energy radiates as Rossby waves into the interior of the northern and southern basins. Wave energy reaches the Indian Ocean by Kelvin waves traveling around the southern tip of Africa. Passing the Indonesian passages, the Kelvin waves eventually reach the Pacific Ocean. Through Rossby wave shedding in the Pacific, the thermocline readjusts on time scale of decades. It was shown (Huang et al. 2000; Goodman 2001; Cessi et al. 2004; Timmermann et al. 2005a) that a shutdown of the AMOC may lead to a deepening of the equatorial thermocline in the eastern equatorial Pacific of 10–40 m. This may be enough to weaken the amplitude of ENSO significantly (Timmermann et al. 2005a).

Using a coupled atmosphere–ocean model of intermediate complexity forced with a freshwater pulse in the northern North Atlantic, Timmermann et al. (2005a) showed that the thermocline anomalies in the Pacific associated with a substantial weakening of the AMOC may lead to a strong suppression of ENSO variability. However, as will be shown in our study here, the oceanic synchronization mechanisms may be overcompensated by the atmospheric bridge generated by Atlantic SST anomalies, which also induces thermocline depth anomalies in the tropical and subtropical Pacific due to Ekman pumping. As will be shown here, through interactions with the annual cycle, a shutdown of the AMOC may even generate an intensification of ENSO, on top of the purely oceanic ENSO suppression mechanism suggested in Timmermann et al. (2005a).

The focus of our study is the impact of an AMOC shutdown on the tropical mean climate in the Pacific, the annual cycle, ENSO, and their interactions. Analyzing waterhosing experiments recently performed with five different state-of-the-art CGCMs, we follow a conceptual framework for ENSO amplitude control outlined by Timmermann et al. (2007). As part of this framework it was proposed that changes of the meridional asymmetry in the eastern tropical Pacific (which can be modulated on long time scales, e.g., by orbital forcing or by a shutdown of the AMOC) change the amplitude of the annual cycle in the eastern equatorial Pacific (Xie 1994). Because of the frequency entrainment mechanism, a weakened annual cycle may lead to an intensification of the ENSO amplitude and vice versa (Chang et al. 1994; Liu 2002; Timmermann et al. 2007). Frequency entrainment is a part of the phase synchronization process (Huygens 1669; Arnol'd 1965; Bak et al. 1985; Pikovsky et al. 2000) and is a common feature of periodically forced nonlinear oscillatory systems. Its presence is a clear manifestation of nonlinear dynamics.

The paper is organized as follows. After a brief description of the five different CGCMs used in this study and of the modeling experiments (section 2), an overview of the performance of the climate model simulations in the tropical Pacific and Atlantic is given in section 3. The global temperature and thermocline response to a shutdown of the AMOC will be studied in section 4. Section 5 addresses the question of how changes in the meridional asymmetry in the eastern tropical Pacific affect the strength of the annual cycle and ENSO. Simulated annual cycle–ENSO interactions will be described in section 6. Section 7 summarizes our main results and section 8 discusses their main implications for the interpretation of multidecadal variability and for paleo-climate dynamics as well as for future greenhouse warming.

2. Model description and experimental design

As part of the Coupled Model Intercomparison Project (CMIP; Collins and the CMIP Modeling Groups 2005; Meehl et al. 2005), waterhosing experiments were conducted under preindustrial or present-day climate conditions (Stouffer et al. 2006). Different CGCMs were forced with a step function–like 100-yr-long freshwater pulse that was applied to the northern North Atlantic (50°–70°N). The response of the climate system to a pulse with an amplitude of 0.1 and 1 Sv (1 Sv $\equiv 10^6$ m^3 s^{-1}) has been described in detail in Stouffer et al. (2006). Some of the models used in our study such as the Community Climate System Model version 3 (CCSM3) do not follow exactly the CMIP waterhosing protocol.

The following model setups (Table 1) were used to study the influence of a substantial AMOC weakening on tropical Pacific climate.

a. GFDL CM2.1

The Geophysical Fluid Dynamics Laboratory (GFDL) Climate Model version 2.1 (CM2.1) is a fully coupled atmosphere–ocean general circulation model developed at the National Oceanic and Atmospheric Administration's (NOAA's) Geophysical Fluid Dynamics Laboratory. The horizontal resolution of the atmospheric model and land model of GFDL CM2.1 is 2° latitude by 2.5° longitude. The atmospheric model has 24 vertical levels with the top at about 3 hPa. It employs a finite-volume dynamical core and uses the preindustrial radiative forcing condition of the year 1860. The oceanic model is based on the GFDL Modular Ocean Model version 4 (MOM4) codes, which use a tripolar grid to avoid the North Pole singularity. The horizontal resolution is 1° in latitude and longitude with enhanced resolution in the meridional direction in the Tropics. The meridional resolution at the equator is ⅓°. There are 50 vertical levels with 22 evenly spaced levels in the top 220 m. The water exchange across the ocean surface is represented in the model with a real water flux. A dynamical–thermodynamical sea ice model with the elastic–viscous–plastic technique to calculate internal ice stresses is used to predict the sea ice. The details of the model configurations, coupling procedure, and performance can be found in Delworth et al. (2006), Gnanadesikan et al. (2006), Wittenberg et al. (2006), and Griffies et al. (2006). The last 200 yr of a multicentury preindustrial model integration are chosen as the control run. In the waterhosing experiment, 1 Sv of external freshwater flux is uniformly added into 50°–70°N of the North Atlantic for 100 yr. Without a global compensation, this freshwater input would add about 9 m of globally averaged sea level over the hosing period. This model does not use any flux adjustments.

b. NCAR CCSM2

The second model analyzed here is the National Center for Atmospheric Research Community Climate System Model version 2.0 (NCAR CCSM2; Kiehl and Gent 2004). Its atmospheric component is the NCAR Community Atmospheric Model (CAM2) with T42 resolution and 26 levels vertically. The ocean model is a version of the Parallel Ocean Program (POP) developed at Los Alamos National Laboratory with 1° resolution and enhanced meridional resolution (½°) in the equatorial Tropics, and with 40 vertical levels. The sea ice model is the Community Sea Ice Model (CSIM4) with elastic–viscous–plastic dynamics, a subgrid-scale thickness distribution, and energy-conserving thermodynamics. The land model is the Community Land Model (CLM2). Although the ocean model is a free surface model, the virtual salt flux is used here for the air–sea freshwater exchanges. The present-day control simulation is integrated for 1000 yr. Here only the model years 500–699 of the control simulation will be analyzed. The hosing experiment is branched from the control run at year 500. The 1 Sv of additional freshwater flux is uniformly distributed in the northern North Atlantic between 50° and 70°N without a global salinity compensation. Therefore, the global mean salinity is not conserved in this hosing experiment and the global mean sea level remains constant.

c. NCAR CCSM3

The CCSM3, developed by NCAR, is used in the low-resolution version suitable for long-term simulations (Yeager et al. 2006). It is a comprehensive atmosphere–ocean general circulation/land surface model with a resolution of T31 in the atmosphere and a variable horizontal resolution in the ocean ranging from 3.75° × (1.8°–0.9°) and increasing toward the Tropics. The ocean model consists of 25 irregularly spaced levels with a relatively fine spacing in the upper ocean. All simulations conducted here refer to a control simulation under perpetual A.D. 1990 conditions (present-day climate setup). The perturbation experiment consists of a strong "triangular" freshwater forcing history in the North Atlantic with freshwater being added between 50° and 70°N. The freshwater forcing increases from 0 to 2 Sv for 100 yr, and then decreases back to 0 Sv during another 100 yr. The global salt balance is satisfied by uniformly removing freshwater from the remaining ocean surface.

TABLE 1. Summary of CGCMs used in this study and their simulated std dev of Niño-3 SST (including annual cycle). The observed Niño SST std dev is 1.25 K (averaged from 1960–2006).

Model	Atmosphere resolution (°)/scheme	Ocean resolution (°)/scheme	CO_2 (ppmv)	Niño-3 SST (K)
GFDL CM2.1	2×2.5, L24	$1/3-1 \times 1$, L50 (MOM4)	286	1.59
HadCM3	2.5×3.75, L19	1.25×1.25, L20	290	1.05
CCSM2	T42, L26	1×1, L40 (POP)	354	1.21
CCSM3	T31	$3.75 \times 1.8 - 3.75 \times 0.9$, L25	354	1.55
ECHAM5-OM1	T31, L19	3×3	280	2.21

d. MPI-OM1

The Max Planck Institute Ocean Model (MPI-OM1) coupled model consists of the atmosphere/land component ECHAM5 (Roeckner et al. 2003) and the ocean/sea ice model MPI-OM (Marsland et al. 2003). The configuration used here is a version of the Intergovernmental Panel on Climate Change Fourth Assessment Report (IPCC AR4) setup described by Jungclaus et al. (2006). Jungclaus et al. (2006) also showed that an improved parameterization of the wind stress calculation in a more recent version of the MPI model results in an improved simulation of the cold bias and the ENSO characteristics. The atmosphere is run at T31 spectral resolution with 19 hybrid levels, and the ocean grid has a resolution of 3° with grid poles moved to Greenland and Antarctica leading to grid sizes from 20 km near Greenland to 375 km in the Pacific. There is no refinement of the grid in the equatorial region. There are 40 unevenly spaced levels in the vertical. The model does not require flux adjustment to maintain a stable preindustrial climate. The waterhosing experiment is started from year 150 of a 1000-yr-long preindustrial control integration by adding instantaneously to the atmospheric flux field, a freshwater flux of 1 Sv distributed over the North Atlantic between 50° and 70°N. The freshwater flux is not compensated by extraction elsewhere (as to simulate the massive disintegration of ice sheets). The waterhosing is kept constant for 100 yr. Thereafter the integration is continued for another 100 yr allowing the MOC to recover.

e. Met Office (UKMO) HadCM3

The Third Hadley Centre Coupled Ocean–Atmosphere General Circulation Model (HadCM3) is described by Gordon et al. (2000). It has a stable control climatology and does not use flux adjustments. The atmospheric component of the model has 19 levels with a horizontal resolution of 2.5 degrees of latitude by 3.75 degrees of longitude. The oceanic component of the model has 20 levels with a horizontal resolution of 1.25 $\times$ 1.25 degrees and employs a scheme to parameterize horizontal mixing of tracers with a variable thickness diffusion parameterization (Wright 1997). Near-surface vertical mixing is parameterized partly by a Kraus–Turner mixed layer scheme for tracers (Kraus and Turner 1967), and a K-theory scheme (Pacanowski and Philander 1981) for momentum. The sea ice model uses a simple thermodynamic scheme including leads and snow cover. Ice is advected by the surface ocean current only. The control run uses preindustrial boundary conditions. The 1-Sv freshwater pulse is evenly distributed over the North Atlantic between 50° and 70°N for 100 yr. The freshwater hosing experiment is continued for another 100 yr, without applying additional freshwater fluxes. These modeling experiments do not employ salinity compensation.

3. Model performance of the control simulations

a. Annual mean state and interannual variability

A comparison of the simulated preindustrial and present-day SST mean states for the five different models and the observations is shown in Fig. 1. Generally, the five different CGCMs simulate the tropical climate mean state and its interannual variability quite realistically.[1] However, there are several features some of these models fail to simulate correctly. As compared to the observations [optimum interpolation SST (OISST) data (Reynolds et al. 2002) and wind stress (Kalnay et al. 1996)], all of the CGCM control simulations are too cold in the western and central equatorial Pacific. This feature is most strongly pronounced in the MPI-OM1 control simulation. In this model the mean thermocline depth, as characterized here by the depth of the 20°C isotherm, is too shallow in the western tropical Pacific, resulting in too-large interannual variabilities throughout the entire tropical Pacific.

In addition to the typical equatorial cold bias, these

[1] It should however be noted that some of the control simulations analyzed here represent preindustrial conditions, rather than present-day conditions.

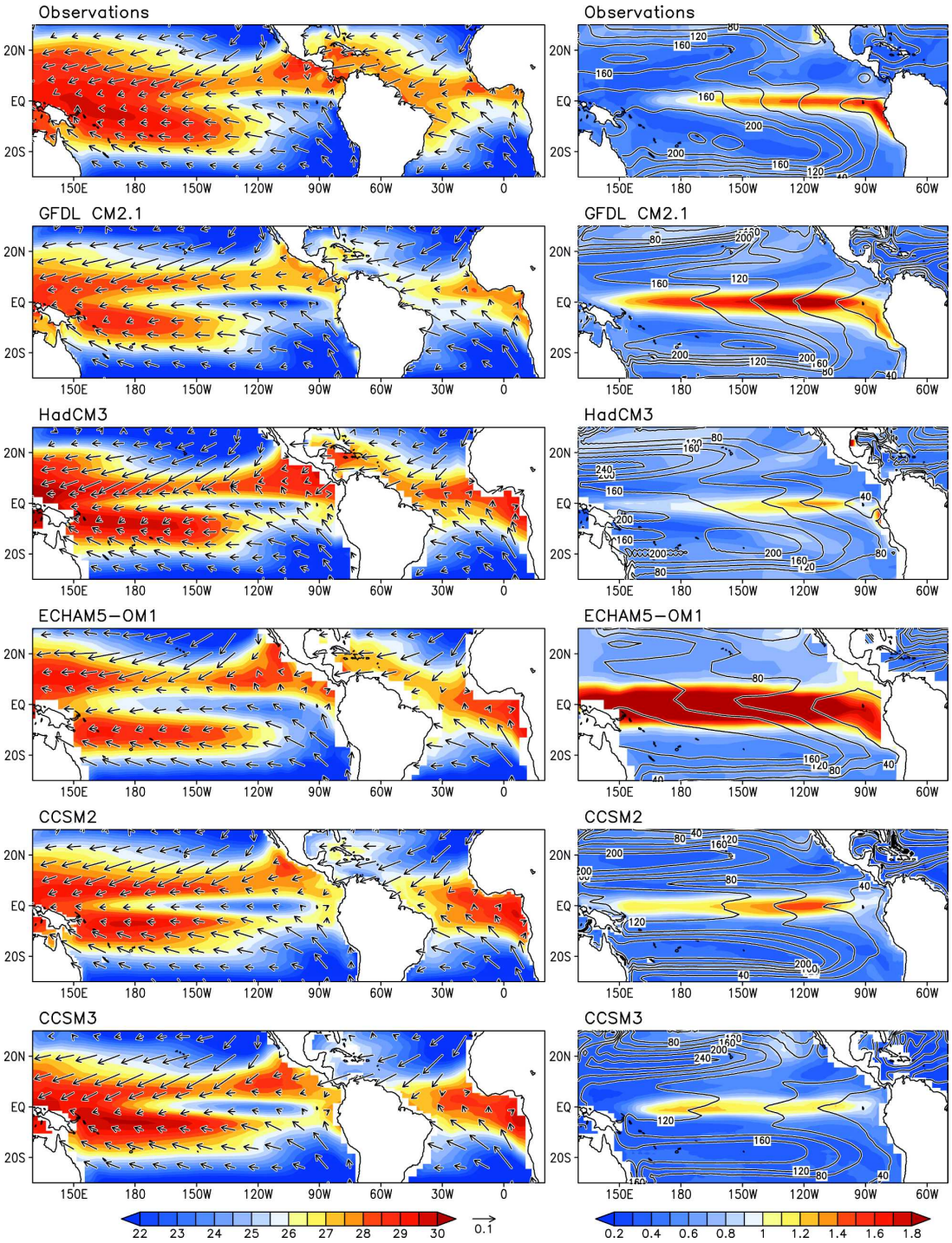

FIG. 1. (left) Observed long-term wind stress (vectors, N m^{-2}) (Kalnay et al. 1996) averaged from January 1948 to March 2005, and (top–bottom) (colors, °C) observed annual mean SST (Reynolds et al. 2002) averaged from December 1981 to 2005, simulated annual mean SST for the GFDL CM2.1 (preindustrial), HadCM3 (preindustrial), MPI-OM1 (preindustrial), NCAR CCSM2 (present-day), and NCAR CCSM3 (present-day). (right) Same as (left), but for the long-term annual mean thermocline depth (contours, m) (Levitus 1994) and the std dev of SST anomalies (colors, K).

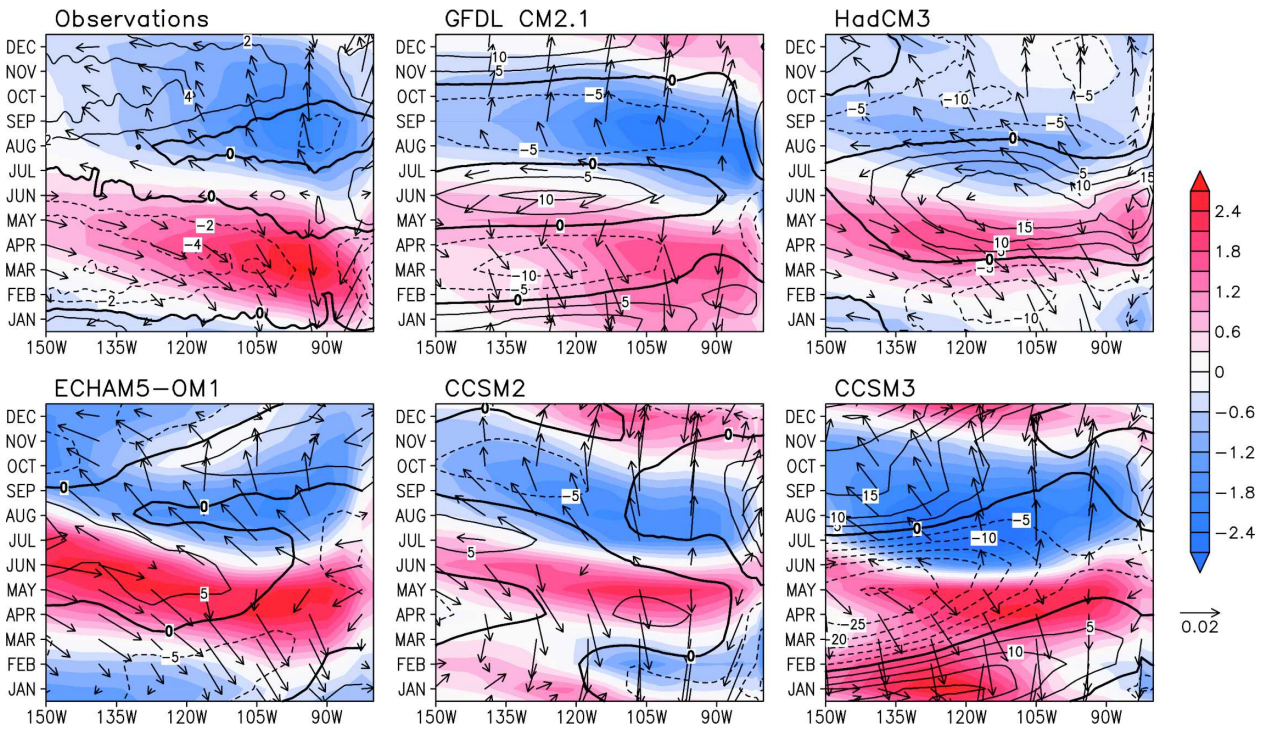

FIG. 2. Hovmöller diagrams of the mean present-day seasonal cycle of Pacific equatorial SST (colors, K) using (top left) the observed SST (Reynolds et al. 2002), wind stress (vectors, N m^{-2}) (Kalnay et al. 1996), and sea level data (contours, cm) (Ducet et al. 2000). A 1-cm increase in SSH roughly corresponds to a 3-m deepening of the thermocline (assuming a 1.5-layer model with a reduced gravity of 0.003 kg m^{-3}). (remaining panels) As in (top left), but for the simulated SST, wind stress, and thermocline depth (depth of the 20°C isotherm) climatologies obtained from the first 100 yr of the control simulations of the GFDL CM2.1 (preindustrial), HadCM3 (preindustrial), MPI-OM1 (preindustrial), CCSM2 (present-day), and CCSM3 (present-day).

model simulations exhibit a warm bias in the southeastern Pacific, which is most strongly pronounced in the CCSM2, CCSM3, and HadCM3 model simulations, whereas it is weakest in the GFDL CM2.1. Different suggestions have been made to explain the warm biases in the upwelling regions, ranging from stratus cloud representations (Philander et al. 1996; Yu and Mechoso 1999; Wang et al. 1999), missing Tsuchyia jets (J. McCreary 2006, personal communication), lack of mesoscale variability (Seo et al. 2006), and overestimation of vertical mixing in coupled models (K. Richards 2006, personal communication). This underestimated meridional asymmetry often leads to the development of an unrealistic double ITCZ in both hemispheres and to the generation of strong semiannual cycles in the eastern equatorial Pacific (see Fig. 2) such as in the CCSM2 and CCSM3 model runs. The reduced meridional cross-equatorial asymmetry also leads to a damping of interannual variability in the southeastern tropical Pacific as documented by the CCSM2, CCSM3, and HadCM3 model simulations.

Typically the general representation of the cold tongue complex and the equatorial annual cycle in CGCMs also influences the fidelity of the model to simulate the position of the ITCZ and the South Pacific convergence zone (SPCZ), the equatorial annual cycle, and ENSO (Fig. 1, right). A too-shallow thermocline in the warm pool as simulated by CCSM3 leads to a variance maximum in the warm pool, in contrast to observations, which show a maximum of the ENSO variance in the eastern equatorial Pacific. In CCSM2 the pattern of maximum ENSO variance corresponds to the area occupied by the tropical Pacific cold tongue. Similar associations can be found for all CGCM simulations analyzed here. The differences between simulated and observed mean state might also have an influence on the sensitivity of ENSO to climate perturbations, such as greenhouse warming or a collapse of the AMOC.

Similar to the southeastern Pacific warm bias, large differences between observations and all of the CGCMs can be found in the tropical Atlantic. None of these models simulates the observed zonal temperature gradient along the equator realistically. All CGCMs analyzed here exhibit too-high temperatures in the eastern tropical Atlantic. Furthermore, as compared to the observations, the GFDL, the CCSM2, and the

CCSM3 model simulations exhibit cold anomalies in the Caribbean that are likely to affect also the cold tongue in the tropical Pacific through atmospheric teleconnections, as will be shown in this study.

b. Equatorial Pacific annual cycle

One key element for the generation of the equatorial annual cycle is the northern position of the ITCZ and the attendant meridional temperature asymmetry around the equator, both of which are partly triggered by the land–sea contrasts in the eastern equatorial Pacific area (Philander et al. 1996) and maintained by air–sea interactions (Xie 1996). The SST asymmetry generates cross-equatorial winds, which in turn cool the southern tropical eastern Pacific by increased evaporation, upwelling, mixing, and cloud-radiative forcing. North of the equator however, the cross-equatorial winds lead to a warming due to reduced evaporation (as compared to the meridionally symmetric state) and reduced mixing. This north–south temperature asymmetry is further amplified by the generation of low-level stratus clouds, which form over the cold waters and lead to increased reflection of solar radiation. The north–south temperature difference in turn generates cross-equatorial winds as a result of the Gill response (Gill 1980). Thanks to the positive air–sea feedbacks, the annual mean ITCZ is kept north of the equator.

With the changing seasons, the north–south SST asymmetry changes as well as the strength of the cross-equatorial trade winds. This provides the seeding for the annual cycle of SST on the equator. However, as will be shown below, the meridional asymmetry is also strongly controlled by the strength of the AMOC. In addition, coupled air–sea interactions (Xie 1994; Li and Philander 1996; Yu and Mechoso 1999) involving evaporative cooling, mixing, and stratus clouds generate a westward-propagating equatorial zonal mode with near-annual frequency that intensifies the annual wind forcing and in turn the westward-propagating equatorial annual cycle of SST. This positive feedback leads to the establishment of a coupled annual cycle in the eastern and central equatorial Pacific. Physical processes responsible for the generation of the annual cycle of SST in the eastern equatorial Pacific are thus somewhat distinct from those that govern the interannual mixed thermocline/SST ENSO mode.

These coupled mechanisms are documented for the observations in Fig. 2 (top left). Weakened trade winds in spring to the west of the maximum warming initiate a westward propagation of the warm water anomaly via reductions of mixing, upwelling, reduced solar insolation, and evaporative cooling. In boreal fall this cycle reverses, driven by the southerly wind component, which originates from the atmospheric response to off-equatorial SST anomalies. Figure 2 shows the observed present-day annual cycle of SST and wind stress and sea level height (annual mean subtracted), and the simulated preindustrial annual cycles for the GFDL CM2.1, HadCM3, and MPI-OM1 and the present-day annual cycle for the CCSM2 and CCSM3 control simulations. The CGCMs apparently have severe problems in reproducing the observed coupled annual cycle of SST and winds realistically. In contrast to the observations, CCSM2 and CCSM3 exhibit a strong semiannual cycle in the eastern equatorial Pacific, owing to the weak mean meridional asymmetry in these model simulations. The phase of the annual cycle is somewhat unrealistic also in the GFDL model and HadCM3, exhibiting an early warming (GFDL CM2.1) or a delayed warming phase in the far eastern equatorial Pacific (HadCM3). While CCSM3 annual cycle of thermocline anomalies involves annual Kelvin wave pulses with magnitudes of up to 25 m, the GFDL model exhibits semiannual thermocline anomalies that seem basically unrelated to the SST anomalies. Thermocline anomalies in MPI-OM1 and CCSM2 are rather small, supporting the notion that the annual cycle of SST in the eastern equatorial Pacific does not primarily involve thermocline dynamics (Xie 1994). The thermocline anomalies in HadCM3 do not show any clear propagation, and their relationship to the winds and SST anomalies is also more complex than for the other CGCMs. Disentangling the annual cycle of the thermocline depth anomalies in terms of wave reflection, off-equatorial Ekman pumping, and other processes (Wang et al. 2000) is beyond the scope of this paper.

4. Global response to AMOC shutdown

The time evolution of the maximum of the meridional streamfunction in the North Atlantic for the five different models is depicted in Fig. 3. For each model, 200 yr of the control simulation are displayed (blue curves) along with 200 yr of the freshwater hosing experiment (red). The long-term mean strength of the AMOC in the control simulations varies between 15 and 22 Sv. In all simulations the strength of the AMOC drops down to 2.5–6 Sv shortly after the onset of the freshwater pulse. The strongly weakened AMOC state will be referred to as the *perturbation state*. The typical time scale for the shutdown of the AMOC is about 20–50 yr, except for CCSM3, which was forced by a linearly increasing and decreasing freshwater flux, suggesting that wave adjustment processes (Johnson and Marshall 2004) play an important role as well as advective processes (Goodman 2001).

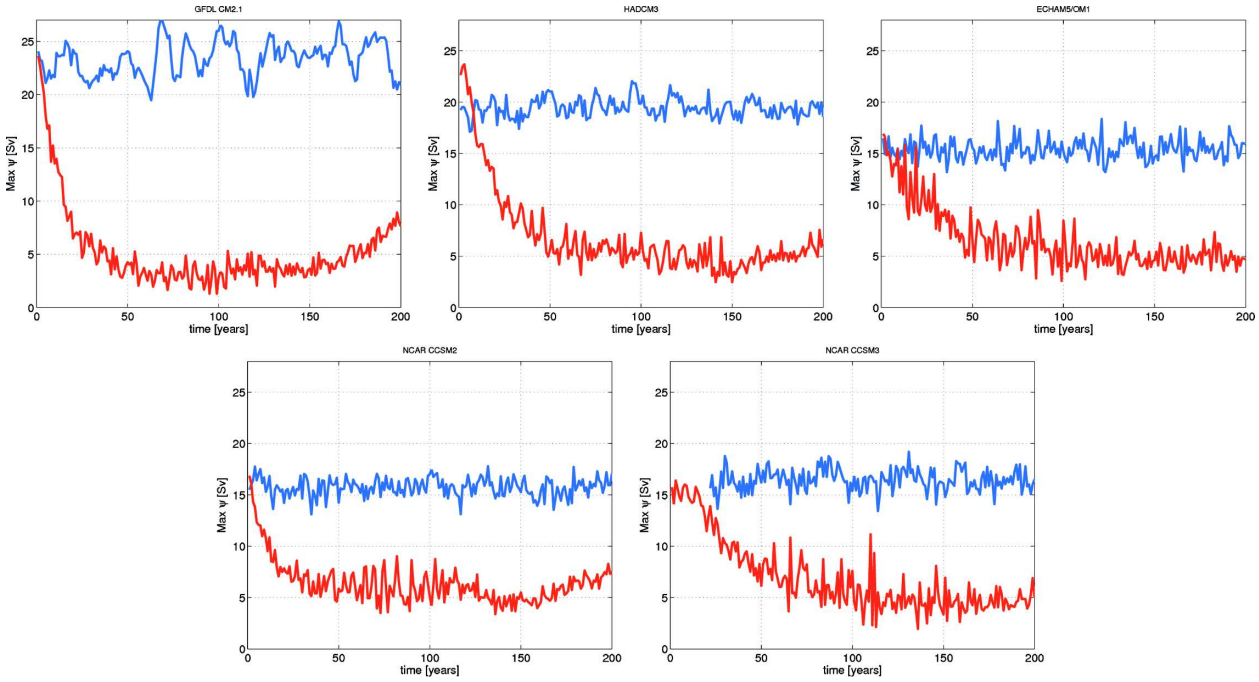

FIG. 3. Time series of the maximum meridional streamfunction in the North Atlantic (Sv) for the five different models and the waterhosing experiment (red) and the control experiment (blue). The initial states for the waterhosing experiments are obtained from different stages of the respective control simulations.

Figure 4 shows the Atlantic and Pacific SST anomaly pattern associated with a perturbation state of the AMOC (averaged difference over the first 100 yr of the perturbation state and the first 100 yr of the control simulation) as simulated by the five CGCMs. We observe the well-known interhemispheric seesaw pattern in SST (Stocker and Johnsen 2003; Knutti et al. 2004), although the simulated temperature anomalies around

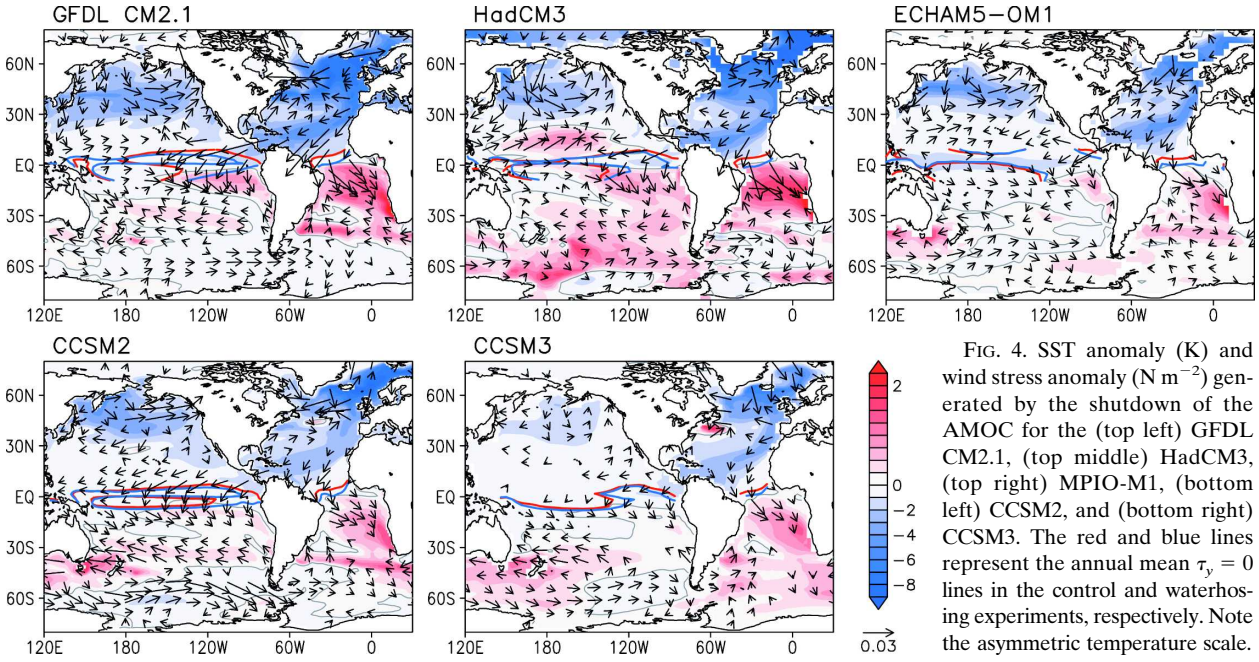

FIG. 4. SST anomaly (K) and wind stress anomaly (N m^{-2}) generated by the shutdown of the AMOC for the (top left) GFDL CM2.1, (top middle) HadCM3, (top right) MPIO-M1, (bottom left) CCSM2, and (bottom right) CCSM3. The red and blue lines represent the annual mean $\tau_y = 0$ lines in the control and waterhosing experiments, respectively. Note the asymmetric temperature scale.

Antarctica are quite small, except for the HadCM3 and the CCSM3 response.

Large positive temperature anomalies can be found in the Benguela current region and can be partly explained in terms of a substantial weakening of the southerly alongshore winds in this area (Fig. 4), which under unperturbed conditions pump cold waters to the surface.

Based on the robustness of these results, we can argue that the Benguela current region might be an optimal site to retrieve proxy records capturing the bipolar seesaw. Analyzing the time evolution of these anomalies more in detail (not shown here) reveals that the cooling starts in the northern North Atlantic and spreads farther south within a few decades until it reaches its full magnitude (typically 50 yr after the beginning of the meltwater pulse). This spreading, which will be studied in more detail in a forthcoming study, involves atmosphere–ocean interactions (Chiang and Bitz 2005), ocean dynamics, and the adjustment of the Hadley circulation (Broccoli et al. 2006). While the adjustment mechanisms are robust in different models, what appears to be fundamental is the requirement for the atmosphere to transport heat into the cooler hemisphere as described by Broccoli et al. (2006).

Figure 4 shows also a significant warming of up to 1°C in the tropical southeastern Pacific, as well as a cooling of the tropical northeastern Pacific by 2°C, consistent with the findings of Zhang and Delworth (2005) and Timmermann et al. (2005b). In the GFDL model, CCSM2, CCSM3, and HadCM3 this pattern is quite distinct from a zonal mode pattern sometimes referred to as a permanent El Niño state. In these model simulations one of the most striking features of the SSTA pattern in the tropical Pacific is the strong meridional structure near the equator, which—superimposed on a meridionally asymmetric mean state of opposite direction—reduces the mean meridional asymmetry across the equator (see Fig. 4). Eventually, during the shutdown phase the warm northeastern tropical Pacific cools, whereas the southeastern Pacific cold tongue complex warms substantially. During the mature shutdown phase, the Pacific temperature gradient across the equator is even reversed in some of the models, leading to a reversal of the mean cross-equatorial trade wind direction (see Fig. 4) and also to a shift of the mean ITCZ to the Southern Hemisphere in some cases. This clearly illustrates that the position of the present-day annual mean ITCZ in these models is not only determined by continental asymmetries and air–sea interactions (Philander et al. 1996), but also by the presence or absence of an AMOC in the Atlantic Ocean (Zhang and Delworth 2005) and the Atlantic–Pacific atmospheric bridge via Central America.

Four out the five CGCMs analyzed here produce a rather consistent picture of changes in the eastern tropical Pacific which projects strongly onto a meridional mode pattern. The simulated tropical Pacific response of MPI-OM1 is qualitatively very different. A substantial weakening of the AMOC in MPI-OM1 generates a permanent La Niña–like pattern (zonal mode) with only weak meridional mode contributions. This will have repercussions also on the sensitivity of the annual cycle and ENSO in this model, as will be shown below.

Atmospheric teleconnections from the tropical Atlantic play a crucial role in generating oceanic and atmospheric anomalies in the eastern tropical Pacific (Dong and Sutton 2002; Zhang and Delworth 2005). In response to the anomalous southward SST gradient in the tropical Atlantic, the Atlantic ITCZ shifts to the south (Fig. 4), forcing westward-propagating atmospheric Rossby waves. The Caribbean cooling and the associated increase in sea level pressure are particularly important in communicating the Atlantic changes to the Pacific across a narrow land corridor of Central America: the intensified northeasterly trades blow over the tropical northeastern Pacific, advecting cold, dry air and enhancing evaporation from the sea surface (Wu et al. 2005). The resultant cooling of the tropical northeastern Pacific will trigger the WES feedback within the Pacific basin, amplifying the southward shift of the Pacific ITCZ and the corresponding warming in the tropical southeastern Pacific. Air–sea interactions may further spread the equatorially asymmetric anomalies to the west (Xie 1996).

While during the AMOC shutdown stages, the thermocline anomalies in the Atlantic exhibit a rather model-independent structure (not shown) with shoaling in the tropical North Atlantic, largely due to surface cooling, and with a deepening in the southeastern Atlantic and the Benguela region, the equatorial Pacific response is less robust (see Fig. 5).

Near the equator it is useful to split the simulated thermocline anomalies conceptually into a zonal mean and a zonal tilt term. In both CCSM2 and CCSM3, the zonal mean equatorial thermocline[2] deepens by several meters. The vertical resolution of the ocean general circulation models might also be an important factor in determining the exact value of the zonal mean thermocline changes. In general, the zonal mean thermocline depth is strongly controlled by the eastern and

[2] The zonal mean equatorial thermocline is taken here as the depth of the 20°C isotherm averaged between 120°E–90°W.

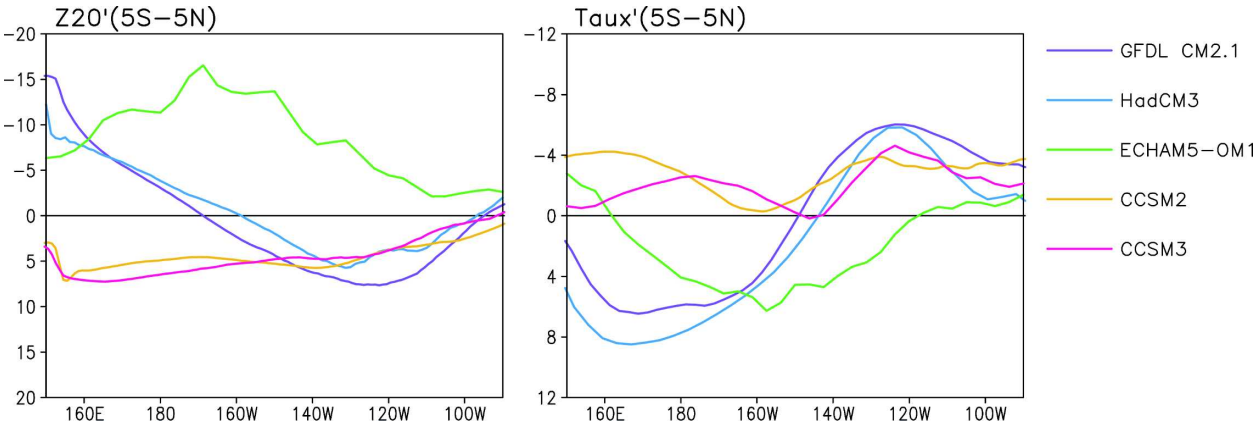

FIG. 5. (left) Thermocline depth anomalies (m) and (right) wind stress anomalies associated with a perturbation state of the AMOC (averaged difference between 200 model years of the waterhosing experiment and the control run). The anomalies are computed as the spatial average between 5°S and 5°N for the GFDL CM2.1 (purple), HadCM3 (blue), MPI-OM1 (green), CCSM2 (yellow), and CCSM3 (magenta). Positive thermocline depth anomalies represent a deepening of the thermocline.

western boundary fluxes and the zonally averaged meridional mass flux divergence. The zonally averaged meridional velocity can be obtained from the changes of the western boundary currents as well as the zonally averaged Sverdrup transport, which in turn is driven by the wind stress curl. For reasons of simplification we will focus here on the effect of the Sverdrup transport. The zonal and temporal mean thermocline depth changes in the waterhosing experiments are partly controlled by the curvature changes of the wind stress, involving the second-order meridional derivative. In fact the deepening of the zonal mean thermocline in CCSM2 and CCSM3 goes along with zonal mean Sverdrup transport convergence (not shown) toward the equator. In MPI-OM1 and HadCM3 the zonal mean thermocline shoals by 8 and 4 m, respectively. This zonal mean shoaling is accompanied by a Sverdrup transport divergence (not shown). The GFDL model simulates a zonal mean thermocline shoaling of 4 m, in spite of a Sverdrup transport convergence. In general, these diagnosed relationships have to be interpreted carefully. We have identified here the zonally integrated mass flux into the equatorial thermocline as the zonal integral of the Sverdrup transport convergence, neglecting changes of the Indonesian throughflow and the fact that the Sverdrup transport is a barotropic transport, rather than a near-surface transport into the thermocline. The large model discrepancies in the simulated zonal mean thermocline depth anomalies can be partly attributed to the fact that even small meridional changes in the position of the wind stress pattern can lead to large changes of the curvature of the wind stress.

The anomalous zonal thermocline gradients on the equator (Fig. 5) can be related to the zonal wind stress changes induced by the AMOC weakening. It can be clearly seen that negative near-equatorial wind stress anomalies in CCSM2 and CCSM3 lead to a deepening of the thermocline anomaly toward the west. The large positive wind stress anomalies west of 150°W simulated in HadCM3 and the GFDL model lead to a shoaling of the thermocline toward the west.

We can summarize that in all CGCMs, except for the MPI model, the eastern equatorial Pacific is deeper during the AMOC perturbation state than under control run conditions. This effect would lead to a weakening of the efficiency of the thermocline feedback, which normally plays an essential role in amplifying ENSO variability. On the other hand three (GFDL, MPI, and HadCM3) out of five models exhibit a zonal mean thermocline shoaling that might help to amplify ENSO variability (Zebiak and Cane 1987).

5. Effect of background state changes on annual cycle and ENSO

Based on the mechanisms that govern the strength of the present-day annual cycle, we expect that a weakening of the meridional asymmetry in the eastern tropical Pacific, such as the one diagnosed in four out of the five CGCM simulations (Fig. 4), will lead to a weakening of the strength of the annual cycle. This behavior is in fact simulated by the CGCM simulations as revealed by the power spectra of the simulated Niño-3 SST time series shown in Fig. 6.

As a result of the AMOC weakening, the strength of the annual cycle reduces substantially in four of the five models (CCSM2, CCSM3, GFDL CM2.1, and

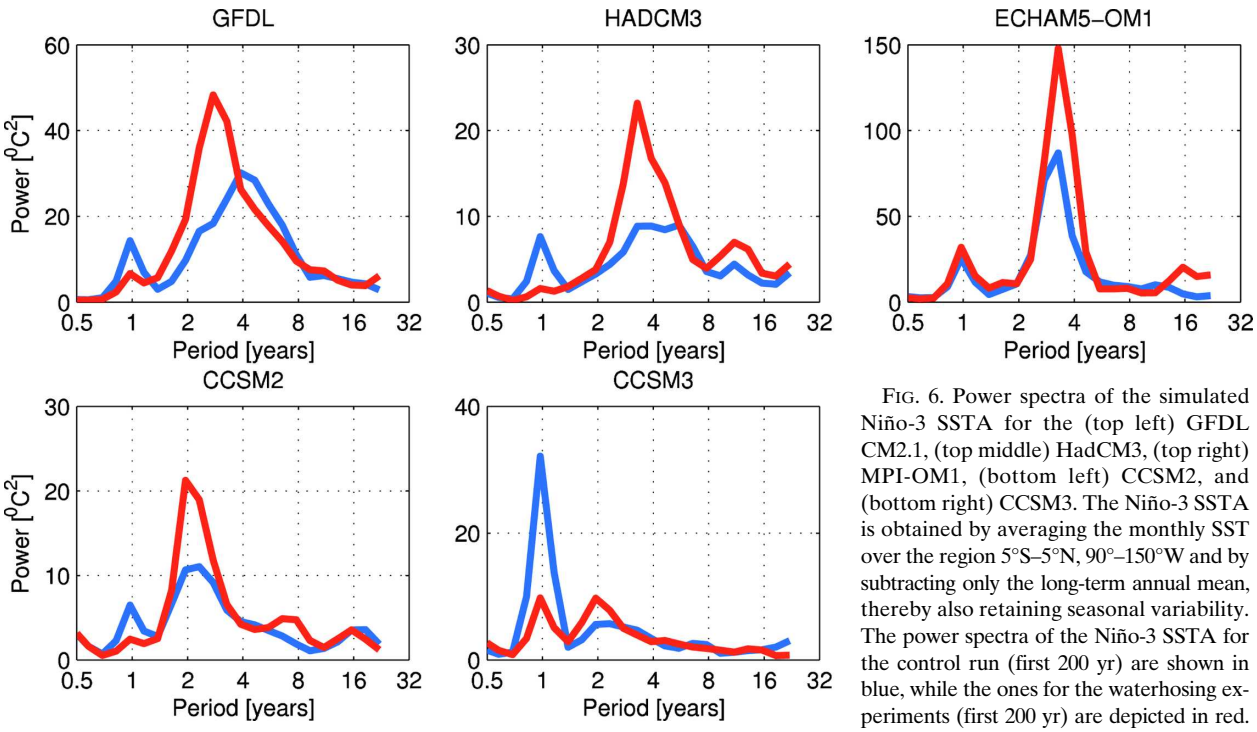

FIG. 6. Power spectra of the simulated Niño-3 SSTA for the (top left) GFDL CM2.1, (top middle) HadCM3, (top right) MPI-OM1, (bottom left) CCSM2, and (bottom right) CCSM3. The Niño-3 SSTA is obtained by averaging the monthly SST over the region 5°S–5°N, 90°–150°W and by subtracting only the long-term annual mean, thereby also retaining seasonal variability. The power spectra of the Niño-3 SSTA for the control run (first 200 yr) are shown in blue, while the ones for the waterhosing experiments (first 200 yr) are depicted in red.

HadCM3). This result supports the notion that the strength of the annual cycle in the eastern tropical Pacific is to a large extent controlled by cross-equatorial winds, which are driven by the meridional SST asymmetry in the eastern equatorial Pacific (Xie 1994) and remotely by the SST conditions in the tropical Atlantic.

To understand the mechanisms for the reduction of the equatorial Pacific annual cycle in four of the five CGCM waterhosing experiments analyzed here, we computed the anomalous seasonal cycle of SST, thermocline depth, and wind stress (see Fig. 7).

Although the mean unperturbed seasonal cycle of the thermocline depth appears unrelated to that of the SST in the control simulations, the anomalous thermocline changes during the waterhosing phase show a clear tendency to be accompanied by temperature anomalies of the same sign.

Anomalous fall to winter cooling near the equator leads to a weak intensification of the annual cycle amplitude in MPI-OM1. There is evidence of an eastward-propagating upwelling Kelvin wave, which is generated by anomalous equatorial easterlies in September. This upwelling signal is likely to influence the SST in fall to winter, thereby amplifying the mean annual cycle (Fig. 2). This works particularly well, because the annual mean thermocline anomaly in the MPI model is already shallower during the waterhosing experiment than in the control run (see Fig. 5). The boreal summer warming around 120°–100°W is probably due to surface processes and in particular due to a reduction of the wind strength in May, rather than due to ocean dynamical processes.

All other CGCMs exhibit a summer to winter warming and springtime cooling, which is opposite to the mean annual cycle of SST and wind stress. In comparison to the MPI-OM1 perturbation experiment, the other four CGCMs simulate a deeper mean thermocline in the eastern equatorial Pacific. Thermocline depth changes triggered by wind stress changes (see GFDL and NCAR models) are not very efficient in modulating the SST due to a weakened thermocline feedback. This leads to an overall lower sensitivity. Springtime cooling in these models is an important contributor to a weakening of the equatorial annual cycle and is induced by strong annual mean northeasterly off-equatorial trade winds associated with a Caribbean positive sea level pressure anomaly and the seasonal modulation of the air–sea coupling strength in the northeastern Pacific, which partly relates to the seasonal cycle of the mean thermocline depth. In fact, such a boreal spring cooling in the eastern equatorial Pacific is also simulated in a regional coupled model of the eastern tropical Pacific in response to a 2°C decrease in tropical North Atlantic SST (Xie et al. 2007).

The power spectra in Fig. 6 clearly show that in all five models ENSO variability is significantly enhanced during the waterhosing phase. One important controlling factor for the amplitude of ENSO is the annual

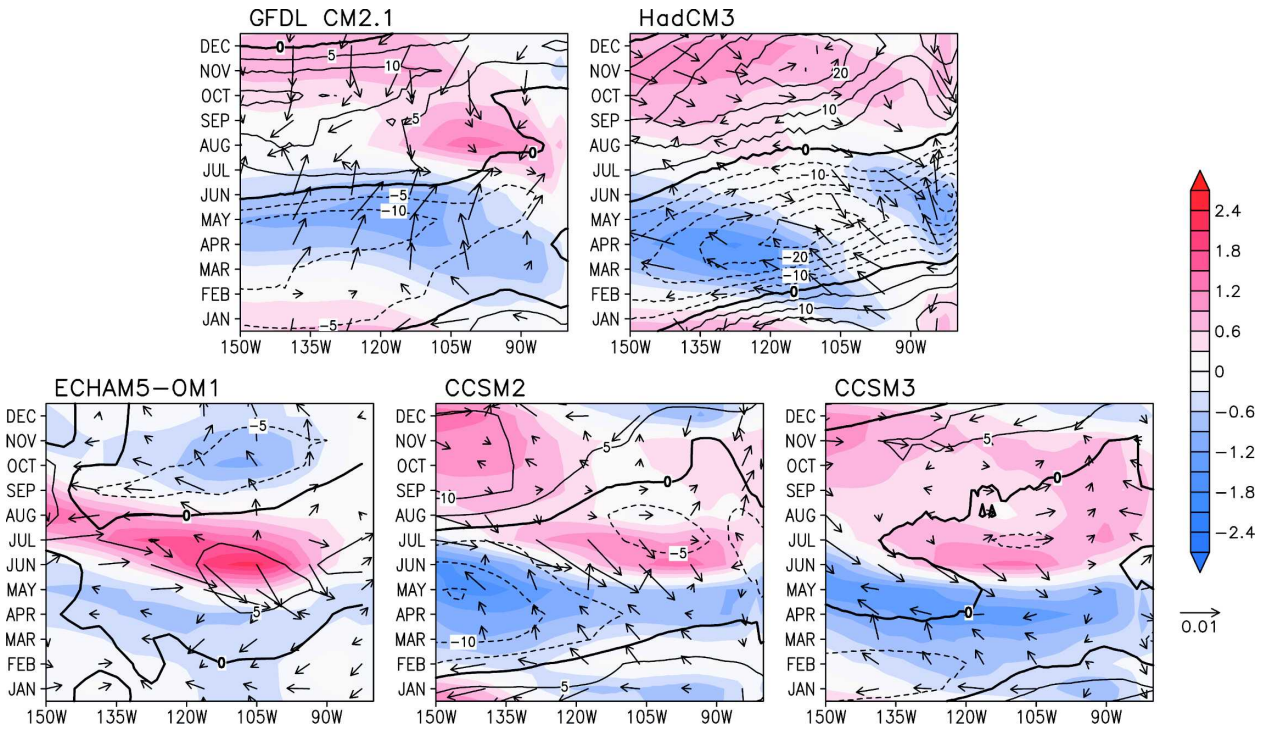

FIG. 7. Hovmöller diagrams of the difference of the simulated equatorial mean seasonal cycle of SST (shading, K), wind stress (vectors, N m^{-2}), and thermocline depth (contours, cm) between the waterhosing experiment (average over first 100 yr) and the control simulation (first 100 yr). The annual mean difference of the respective fields was removed prior to the analysis.

mean background state climate (thermocline depth, mean SST, zonal winds, coupling strength, etc.; Zebiak and Cane 1987). Another mechanism is ENSO's interaction with the annual cycle through the nonlinear frequency entrainment process described in Liu (2002) and Timmermann et al. (2007).

As documented in Fig. 5, the zonal mean equatorial thermocline depth averaged from 120°E and 90°W shoals in the GFDL model, HadCM3, and MPI-OM1 by 4, 3.7, and 8 m, respectively. According to idealized modeling studies (Fedorov and Philander 2000), such a thermocline shoaling might lead to an increase of ENSO instability for those models that exhibit a rather shallow zonal mean thermocline. In our case, only MPI-OM1 has a very shallow zonal mean thermocline (90 m) and the ENSO intensification in this model can be readily explained in terms of the linear theory of Fedorov and Philander (2000). Both the GFDL model and HadCM3 on the other hand have a rather deep zonal mean thermocline (125–130 m) and strong zonal mean winds. Their thermocline depth anomaly pattern under waterhosing conditions is associated with a reduction of the mean thermocline tilt. The linear theory of Fedorov and Philander (2000) is not directly applicable to this situation. Furthermore, the results of Fedorov and Philander (2000) are based on a two-strip model that is not capable of capturing the effect of meridional thermocline and wind asymmetries.

To quantify the effect of the spatially inhomogeneous thermocline, temperature, and wind anomalies (annual mean and anomalous seasonal cycle changes) on the ENSO variance in more detail, a series of sensitivity experiments using an intermediate anomaly-coupled ENSO model [Zebiak and Cane 1987 (ZC) model] is conducted. The ocean model uses a 1.5-layer reduced gravity model, a surface layer model capturing frictional processes and the Ekman layer, and an equation for the mixed layer temperature anomalies. The atmospheric model solves the first baroclinic mode equations on an equatorial beta-plane (Gill 1980) iteratively. The iterative procedure generates some atmospheric noise and subsequently ENSO irregularity. The intermediate model is used in the anomaly coupling mode, that is, prognostic equations are solved for the anomaly with respect to a given annual mean background state—in our case the observational background state for the currents, the mean thermocline depth, the mean temperature, and the winds plus an additional perturbation capturing the effect of an AMOC weakening on the tropical climate.

To obtain the background state perturbations, we used the tropical Pacific SST difference (Fig. 4) be-

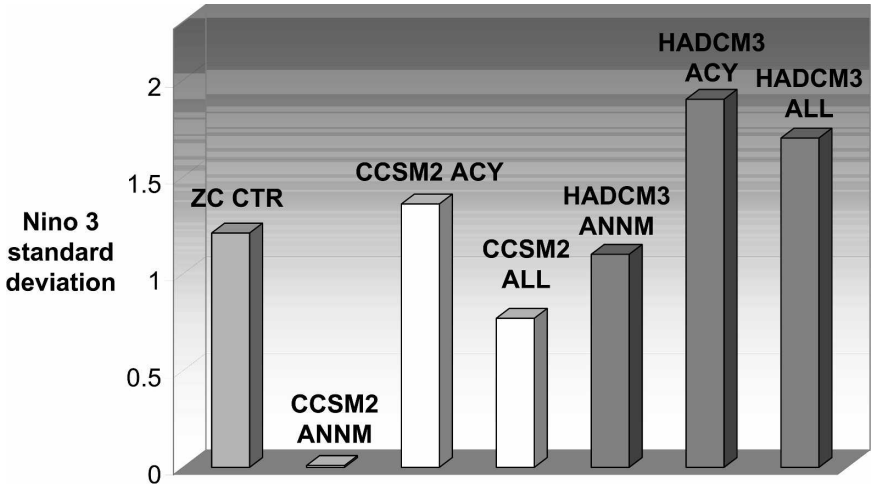

FIG. 8. Std dev of simulated Niño 3 SSTA (K) using the ZC model background state (ZC CTR); the annual mean anomaly of the CCSM2 waterhosing experiment of wind, thermocline, and SST (CCSM2 ANNM); the anomalous seasonal cycle of the CCSM2 waterhosing experiment of wind, thermocline, and SST (CCSM2 ACY); the anomalous seasonal cycle plus background state of the CCSM2 waterhosing experiment of wind, thermocline and SST (CCSM2 ALL); the annual mean anomaly of the HadCM3 waterhosing experiment of thermocline depth only (HadCM3 ANNM); the anomalous seasonal cycle of the HadCM3 waterhosing experiment of thermocline depth only (HadCM3 ACY); and anomalous seasonal cycle plus background state anomaly of the HadCM3 waterhosing experiment of thermocline depth only (HadCM3 ALL).

tween the AMOC perturbation state in the NCAR CCSM2 and the control state as a forcing for the ZC model. Subsequently surface wind and wind divergence background state anomalies are computed from the coupled intermediate model. These surface winds are used to force the 1.5-layer ocean model to calculate the surface layer currents, upwelling, and thermocline depth. Eventually, the diagnosed anomalies for SST and the computed anomalies for surface wind, surface wind divergence, surface layer currents, upwelling velocity, and thermocline height anomalies are added onto the observational present-day background state of the ZC model. This procedure has been done for the annual mean background state change (ANNM) in the tropical Pacific corresponding to a collapsed AMOC state, as well as for the anomalous annual cycle (ACY). A multicentury simulation is performed with the ZC model adding the background state perturbations ANNM and/or ACY to the observed present-day seasonally varying background state. Figure 8 shows the standard deviation of the Niño-3 SSTA simulated by the ZC model for the present-day control state, for the ANNM simulation, capturing the annual mean background state change of the CCSM2 model, the ACY experiment, and the ANNM+ACY (ALL) experiment.

The annual mean background state changes (ANNM) lead to a weakening—and actually a shutdown—of ENSO activity (Fig. 8), in consistency with the results of Timmermann et al. (2005a). This can be mostly attributed to the overall zonal mean thermocline deepening simulated by the CCSM2 simulation (see Fig. 5) as well as to changes of the meridional advection of heat due to the symmetric SST structure (Fig. 3). Apparently the annual mean background state changes cannot explain the observed ENSO intensification observed in CCSM2 (Fig. 6). However, the annual cycle background state changes (ACY) lead to an intensification of ENSO variability in the intermediate ENSO model, in consistency with the results shown in Fig. 6. Figures 6 and 7 clearly show that in CCSM2 the annual cycle strength due to the AMOC collapse reduces substantially. Hence, we can conclude from this intermediate model experiment that a weakening of the annual cycle background state forcing might be an important mechanism to intensify ENSO variability.

To understand the effect of the more dipolar thermocline anomaly structure simulated, for example by HadCM3 (Fig. 5) on ENSO in a more quantitative way, we perturbed the ZC model thermocline depth background state directly by the annual mean (HadCM3 ANNM) and/or seasonal cycle change (HadCM3 ACY) of the tropical thermocline depth field diagnosed from the HadCM3 waterhosing and control simulation. Figure 7 clearly reveals that the anomalous annual cycle projecting on an overall weakening of the mean annual cycle of thermocline depth is a booster for ENSO vari-

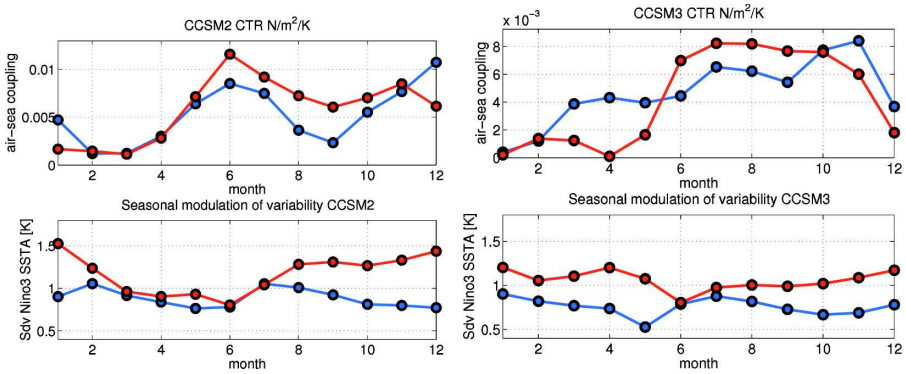

FIG. 9. (top) Monthly regression between zonal wind stress in the central Pacific (averaged over 5°S–5°N, 170°E–140°W) and the Niño-3 SSTA obtained from (left) CCSM2 and (right) CCSM3. Unit is N m^{-2} K^{-1}. (bottom) Monthly std dev (K) of the Niño-3 SSTA for the two models. Blue curves represent the first 100 yr of the control simulation. Red curves are obtained from the first 100 yr of the waterhosing experiments.

ability, whereas the annual mean change of the thermocline, which is characterized by a deepening in the east and a shoaling in the west (Fig. 5), leads to a reduction of ENSO. Both effects together (HadCM3 ALL) can explain a net amplification of ENSO, as compared to the ZC control simulation.

Based on our intermediate model simulations using the Zebiak and Cane (1987) intermediate ENSO model, we can conclude that the zonal mean equatorial thermocline deepening as simulated by CCSM2 and CCSM3, as well as the decrease in thermocline tilt simulated by HadCM3 and GFDL CM2.1, lead to a weakening of ENSO variability—in contrast to Fig. 6. While the MPI-OM1 thermocline shoaling in the entire cold tongue can explain the ENSO intensification in a linear framework (Fedorov and Philander 2000), other nonlinear mechanisms involving the annual cycle need to be invoked to explain the ENSO intensification in CCSM2, CCSM3, GFDL CM2.1, and HadCM3.

6. Effect of annual cycle changes on ENSO

Here we focus on the four different models (GFDL CM2.1, CCSM2, CCSM3, and HadCM3) that exhibit a weakening of the annual cycle and an accompanying intensification of ENSO amplitude during the collapsed AMOC period.

Under present-day conditions the seasonal dependence of the equatorial air–sea coupling strength is an important modulator for ENSO activity (Zebiak and Cane 1987; Tziperman et al. 1997). The coupling strength is controlled by many different factors, which include both atmospheric and oceanic processes. In boreal spring, the ITCZ is close to the equator, which leads to large convergent and upward motion of air, heating the atmosphere via latent heating and moisture condensation. Interannual anomalies in this season will hence experience an enhanced Bjerknes feedback. On the other hand, zonal SST gradients as well as equatorial upwelling are relatively weak, thereby resulting in less efficient zonal and vertical advection in the equatorial ocean, respectively. As can be seen from Fig. 2 (top left), during the spring season the equatorial thermocline is shallower, which might lead to an enhancement of the thermocline feedback (Galanti et al. 2002), thereby enhancing the effect of a wind stress anomaly on the SST. The seasonal competition between the thermocline outcropping feedback and the wind convergence feedback is quite delicate. Small shifts in the background state can lead to significant changes of the seasonality of the air–sea coupling strength. Other effects on the coupling strength that are neglected here are changes of the thermocline sharpness (Timmermann et al. 1999a) and changes in the interaction between intraseasonal wind noise and ENSO (Eisenman et al. 2005; Jin et al. 2007).

To diagnose changes of the air–sea coupling strength due to the weakened AMOC state, we diagnosed the atmospheric sensitivity (Timmermann et al. 1999a) from the monthly stratified regression between zonal wind stress averaged over the central Pacific (170°E–140°W) and the Niño-3 SSTA.[3] The results are depicted in Fig. 9.

For clarity we just focus on CCSM2 and CCSM3. In both models an increase of the summer coupling atmospheric sensitivity can be observed that is accompanied

[3] Here the assumption is made that the main response patterns in the tropical Pacific remain stable.

by a variance increase of the simulated eastern equatorial Pacific temperatures in boreal winter. During the AMOC perturbation state interannual anomalies can grow faster during summer, leading to larger mature El Niño or La Niña events in winter. While similar features can be observed (not shown) also for the GFDL model, the variance changes in HadCM3 happen throughout the year (not shown) without considerable changes of the atmospheric sensitivity.

Attempts to understand why the summer air–sea coupling strength is enhanced for the weakened AMOC state were hampered by the fact that the seasonal modulation of the sensitivity is determined by the wind convergence feedback, the thermocline outcropping nonlinearity, and the strength of zonal and vertical SST gradients as well as other factors. Our analysis of the wind convergence feedback (Zebiak and Cane 1987; not shown) has revealed that the GFDL model, CCSM2, and CCSM3 simulate an enhanced spring to summer wind divergence near the equator, which would in fact weaken the air–sea coupling strength in contrast to Fig. 9. On the other hand these models simulate a shallower eastern equatorial thermocline during the boreal spring to summer (Fig. 7), which might lead to an enhancement of the air–sea coupling trough an increased efficiency of the thermocline feedback. A more in-depth analysis of these feedbacks is very complicated and exceeds the scope of our paper.

As mentioned in the introduction there is ample evidence from CGCM simulations (Guilyardi 2005; Timmermann et al. 2007) as well as from observations (Gu and Philander 1995) that the strength of ENSO can be anticorrelated with the strength of the annual cycle in the eastern equatorial Pacific. This can be interpreted in terms of the nonlinear frequency entrainment concept described in Bak et al. (1985), Chang et al. (1994), and Liu (2002). The main idea is that ENSO is a nonlinear oscillator that is periodically forced by the annual cycle in the eastern equatorial Pacific with a frequency that is incommensurate with its own eigenfrequency. For a weak annual cycle, ENSO maintains its eigenfrequency, whereas for a very strong annual cycle, ENSO's frequency is completely entrained into the forcing frequency and the interannual variance drops (Liu 2002). For a moderate annual cycle strength nonlinear resonances between ENSO and the annual cycle can occur in which ENSO frequency may become a rational multiple of the annual cycle frequency. Near certain thresholds, the selection of a single frequency may become more and more difficult and ENSO can jump between different nonlinear resonances, possibly generating chaotic vacillations. This can be achieved either via the period-doubling bifurcation route to chaos (Chang et al. 1994) or through the quasi-periodic route to chaos (Tziperman et al. 1994). To adopt these types of idealized concepts to the tropical Pacific we have to note, however, that the true forcing is the equatorial semiannual and the off-equatorial top-of-the-atmosphere insolation. The annual cycle of winds is already a result of tropical air–sea interactions and can respond to interannual variability as well as the other way around, thereby complicating the interpretation.

Clearly, more work needs to be done to understand the interaction between the annual cycle and ENSO both in observations and CGCMs in more physical terms.

7. Summary

Our statistical analysis of the CGCM waterhosing simulations focused on five different CGCMs (GFDL CM2.1, NCAR CCSM2, NCAR CCSM3, MPI-OM1, and UKMO HadCM3). In all of these model simulations, a collapse of the AMOC generates the Atlantic seesaw pattern of SSTA, which triggers a large-scale atmospheric response. This atmospheric response is associated with an intensification of the northern hemispheric trade winds in the Atlantic and a large anomalous anticyclonic surface circulation in the Caribbean and its surroundings, as well as a southward displacement of the ITCZ. Partly through the positive WES feedback and partly through large-scale changes of the meridional heat transport, a negative SSTA is generated in the northern tropical Atlantic, whereas the southern Atlantic experiences a warming. This meridional asymmetry weakens the trade winds further (Gill 1980), thereby contributing to the positive WES feedback. Although the South American continent is shielding somewhat the transmission of atmospheric anomalies from the Atlantic to the tropical Pacific, wind anomalies can easily cross Central America, thereby triggering SST anomalies in the northeastern tropical Pacific.

Furthermore, the large-scale cooling in the northern Pacific is also contributing to an overall strengthening of the Hadley cell and a trade wind intensification, which can result in a southward displacement of the ITCZ in the Pacific and further cooling of the northeastern tropical Atlantic. Because of a southward shift of the Pacific ITCZ, consistently simulated in all of the CGCM waterhosing experiments analyzed here, the southeastern tropical Pacific is warming. Ultimately, a reduced meridional asymmetry is established that leads to a weakening of the annual cycle in the case of the GFDL model, CCSM2, CCSM3, and HadCM3. Here we concluded that the weakening of the tropical Pacific

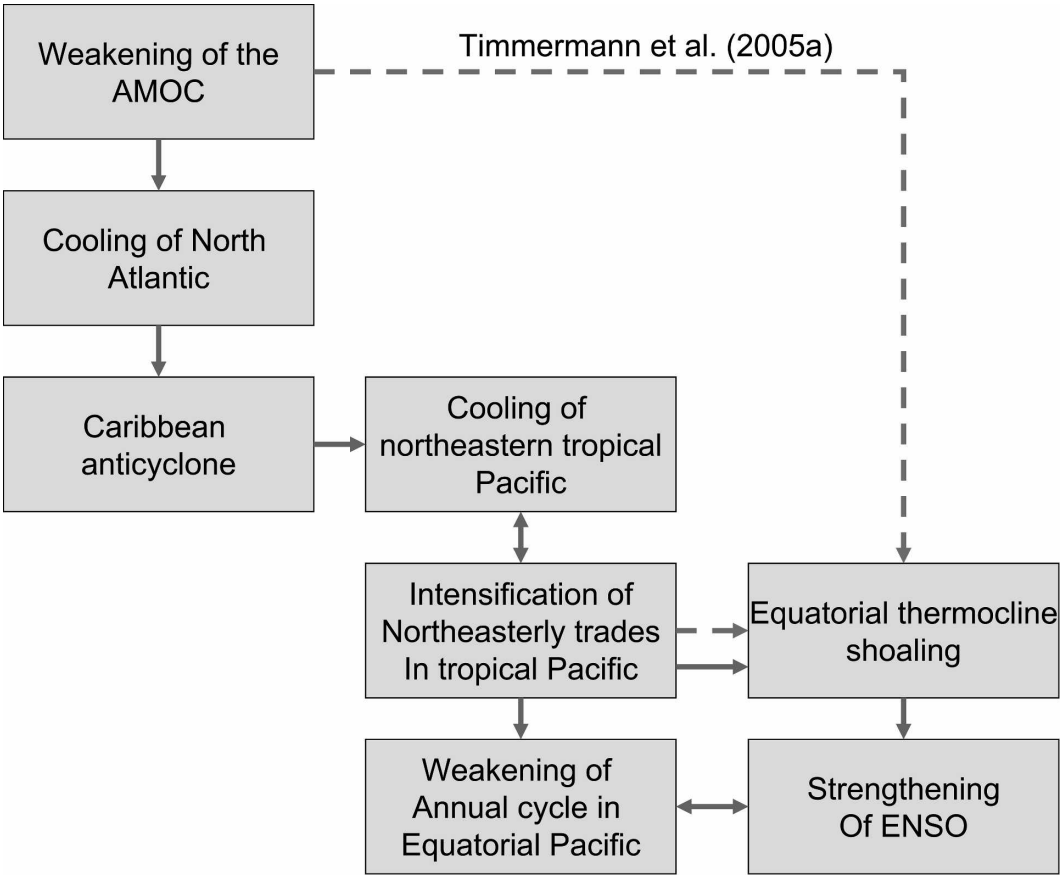

FIG. 10. Schematic illustration of the influence of shutdown of the AMOC on the mean state of the eastern equatorial Pacific, the annual cycle, and ENSO. Solid lines represent a positive correlation, while dashed lines represent a negative relationship.

annual cycle in the GFDL, UKMO, and NCAR models most likely causes an intensification of ENSO. This behavior is reminiscent of the frequency entrainment mechanism and relates to enhanced boreal summer air–sea instability. For these models linear instability arguments (Fedorov and Philander 2000) are unsuitable to explain the diagnosed ENSO intensification. In the MPI model a significant zonal mean thermocline shoaling of about 5–20 m is simulated, which leads to an intensification of the annual cycle in the eastern Pacific and of ENSO in accordance with linear theory. This indicates that the frequency–entrainment concept adopted here to explain the ENSO behavior of the other models is not a universal scenario but strongly depends on the existing background conditions changes and in particular on the simulated the thermocline depth anomalies.

A summary sketch of the diagnosed processes leading to an ENSO intensification during an AMOC collapse is depicted in Fig. 10.

8. Discussion

The results of this study may be relevant also for our understanding of the multidecadal variability of ENSO activity during the twentieth century. Dong et al. (2006) present evidence that variations in SST associated with the Atlantic Multidecadal Oscillation (AMO; e.g., Kerr 2000) can modulate ENSO activity. The AMO, which is thought to be related to multidecadal fluctuations of the AMOC (e.g., Delworth and Mann 2000), was in a negative phase from the mid-1960s to the 1990s, characterized by an anomalously cold North Atlantic and warm South Atlantic, and this period was associated with strong ENSO variability (see Fig. 11) and a reduced annual cycle of SST in the eastern tropical Pacific.

The positive phase of the AMO from the mid-1930s to the late 1960s was associated with an intensified annual cycle and weak ENSO variability (Fig. 11). The observational finding is consistent with our main hy-

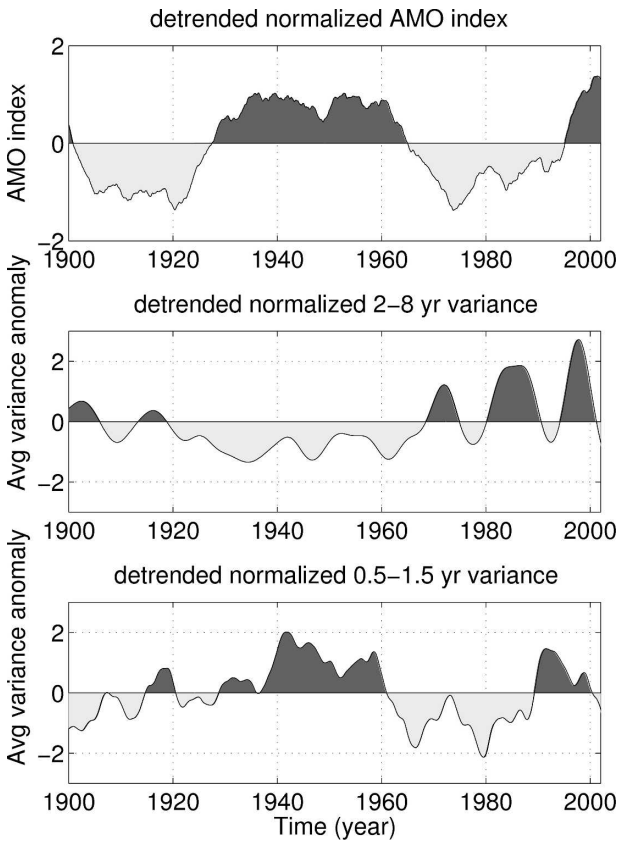

FIG. 11. (top) Low-pass filtered and detrended observed AMO SST index; (middle), (bottom) observed annual and interannual variance anomaly of Niño-3 SST, obtained from the wavelet variance integrated over the periodicity bands of (middle) 2–8 yr and (bottom) 0.5–1.5 yr, respectively. All time series were normalized by their respective std dev. The AMO index was calculated by averaging annual mean SST observations (Rayner et al. 2003) over the North Atlantic region from 0°–60°N.

pothesis that multidecadal changes in the North Atlantic temperature modulate both the annual cycle and ENSO in the tropical Pacific.

Dong et al. (2006) reproduced the relationship between ENSO and the AMO qualitatively in idealized regional coupled experiments where Atlantic SSTs were prescribed to simulate positive and negative phases of the AMO, suggesting that ENSO activity is sensitive to changes in the AMOC. The multimodel results presented in our study are (with the exception of MPI-OM1) in that sense consistent with the results of Dong et al. (2006). Dong et al. (2006); this suggest that eastward-propagating thermocline anomalies play an important role in modulating ENSO activity on multidecadal time scales. This hypothesis is not directly confirmed by the analysis of the HadCM3 waterhosing experiment. While the anomalous seasonal cycle of thermocline depth anomalies shoals in boreal spring (Fig. 7), the absolute thermocline depth anomaly does not change compared to the control simulation. Furthermore, the SST/thermocline as well as the wind stress/SST sensitivities, both contributing to the coupling strength, do not change significantly as a result of the AMOC perturbation.

It should be noted here that tropical Atlantic SST variations associated with the AMO are much smaller (typically of the order of 0.3°C) than those associated with a near collapse of the AMOC (typically of the order of 3°–6°C; see Fig. 4). Given that in both cases we observe a significant change of the ENSO variance, the question can be raised whether the simulated tropical Pacific response to tropical Atlantic forcing is perhaps strongly underestimated. Analyzing the covariability of ENSO and the AMO in CGCMs on multidecadal time scales will help to interpret the short observational record with more confidence. In fact, recent CGCM studies have found that the periodicity of simulated interdecadal "ENSO" amplitude modulations is similar to that of the simulated meridional overturning variations in the North Atlantic (Knutson et al. 1997; Timmermann et al. 1999b; Timmermann 2003).

The potential predictability of the strength of the Atlantic meridional overturning circulation on time scales of a few years to decades (Griffies and Bryan 1997; Grötzner et al. 1999; Latif et al. 2006) might also translate into a potential long-term predictability of the amplitude of the ENSO mode. This would be a type of regime predictability (predictability of the probability distribution of ENSO or of its higher-order statistical moments; Timmermann and Jin 2006), which may have many very interesting societal implications.

Black et al. (1999) reported evidence that multidecadal variations of the interhemispheric SST contrast in the Atlantic have an influence on riverine input into the Cariaco Basin, thereby supporting the proposed link between the AMO and the position of the Atlantic ITCZ on multidecadal time scales. Furthermore, on millennial time scales the hydrological paleo-proxy reconstructions from the Cariaco Basin (Lea et al. 2003), the Indian Ocean (Ivanochko et al. 2005), the western tropical Pacific (Stott et al. 2002), and the eastern tropical Pacific (Koutavas and Lynch-Stieglitz 2004) indicate that the ITCZ was displaced southward during the Heinrich events in the northern North Atlantic. Heinrich events are believed to represent glacial ice sheet instabilities that have triggered major reorganizations of the AMOC (Hemming 2004). Paleo-evidence for our hypothesis controlling changes of the annual cycle and ENSO might come from fossil corals that lived during Heinrich events and that capture interannual variability associated with ENSO (Corrège et al. 2000; Tudhope et

al. 2001). In such records the ratio between recorded interannual variability and the annual cycle strength might be an important indicator for the frequency entrainment mechanism outlined here. Paleo-evidence for enhanced decadal to interdecadal variability in the southeastern Pacific was recently reported using high-resolution cores from off the coast of Peru during the period 12–10 ka B.P. (the Younger Dryas) and the Heinrich event I (see Fig. 9; Rein et al. 2005). It should however be noted that the estimated variance changes of this record need to be normalized by the sedimentation rate. The findings of Rein et al. (2005) are indicative of changes of the eastern tropical variability during major reorganizations of the AMOC. Whether the inferences from Rein et al. (2005) can be adopted to interpret ENSO changes during collapsed AMOC states still remains to be shown. Furthermore, the effect of orbitally driven insolation changes on ENSO (Clement et al. 1999; Timmermann et al. 2007) might further complicate the interpretation of high-resolution tropical records.

The impact of an anticipated anthropogenic greenhouse warming on the AMOC has been the subject of many studies (e.g., Dixon et al. 1999). Most recent CGCM studies (Gregory and et al. 2005; Schmittner et al. 2005) suggest that a doubling of atmospheric CO_2 might lead to a weakening of the strength of the meridional overturning in the North Atlantic by 10%–50%. According to our study, a 50% decrease might already lead to substantial changes of the meridional temperature gradient in the eastern equatorial Pacific and hence to changes of the annual cycle and ENSO. However, it should also be noted that there are other processes internal to the Pacific that modulate the amplitude of ENSO under greenhouse warming conditions, such as changes of the thermocline sharpness, westerly wind burst activity, air–sea coupling, and zonal thermocline gradients. Recent assessments of these internal Pacific effects in multimodel ensembles reveal that the ENSO response to greenhouse warming is highly model dependent (Guilyardi 2005; Philip and van Oldenborgh 2006; Merryfield 2006).

The waterhosing experiments made a good case that the AMOC is an important factor for establishing the meridional asymmetry in Pacific/Atlantic climate. However, the AMOC is probably not the only factor; many TOGA-forced coupled models still have problems in keeping the Pacific ITCZ north of the equator even though observed SST is prescribed outside the tropical Pacific. The shape and topography of the continents and air–sea interactions are still important (Philander et al. 1996). Because latitudinal asymmetry is weak to begin with in some CGCMs, an AMOC shutdown may be enough to destroy this weak asymmetry, as shown here. In reality, the initial climatic asymmetry in the Pacific and Atlantic may be much stronger and probably harder to reverse.

As documented by a recent analysis of CMIP waterhosing experiments (Stouffer et al. 2006), the strength of the simulated present-day AMOC in different CGCMs varies substantially. While the CCC CGCM2 has a mean overturning strength of 14 Sv, the GFDL CM2.1 has a magnitude of 24 Sv. As explained above, these differences may also translate into differences in the simulation of tropical Pacific climate, including the cold tongue, the annual cycle, ENSO, and ENSO decadal variability. Systematic biases in the Pacific may be related to systematic modeling biases in the Atlantic. Further research has to be done to understand these SST bias teleconnections between the ocean basins.

We are aware that our study raises probably more questions than it answers. Questions to be addressed in future research are:

- How exactly does the nonlinear frequency entrainment mechanism for ENSO work physically?
- Why is there such an inconsistency between models for the simulated Pacific thermocline depth anomalies?
- What is the role of topographic features in Central America to link northern tropical Atlantic SST anomalies with the tropical Pacific climate?

Further research needs to be done to translate the results from this study into a better understanding of ENSO's multidecadal variability and its sensitivity to a future weakening of the AMOC as projected by some CGCMs (Schmittner et al. 2005).

Acknowledgments. A. Timmermann and S.-P. Xie are supported by the Japan Agency for Marine-Earth Science and Technology (JAMSTEC) through its sponsorship of the International Pacific Research Center. T. F. Stocker was partly supported by the IPRC visitor program. A. Clement received funding from the NSF Paleoclimate Program (ATM0134742). The support of the European Union's Framework Programme VI via the DYNAMITE project (Contract 003903) is also acknowledged. SIA was supported by Grant R01-2006-000-10441-0 from the Basic Research Program of the Korea Science and Engineering Foundation and the Brain Korea 21 project. CCSM3 simulations were performed at CSCS Manno. TFS and MR acknowledge support by the Swiss National Science Foundation through NCCR Climate. We thank Tony Broccoli, Andrew Wittenberg, and Rich Gudgel for the constructive comments on an earlier version of the manuscript.

REFERENCES

Arnol'd, V., 1965: Small denominators. I: Mappings of the circumference onto itself. *Amer. Math. Soc. Trans.,* **46,** 213–284.

Bak, P., T. Bohr, and M. Jensen, 1985: Mode locking and the transition to chaos in dissipative systems. *Phys. Scripta,* **T9,** 50–58.

Black, D., L. Peterson, J. Overpeck, A. Kaplan, M. Evans, and M. Kashgaraian, 1999: Eight centuries of North Atlantic Ocean atmosphere variability. *Science,* **286,** 1709–1713.

Blunier, T., and Coauthors, 1998: Asynchrony of Antarctica and Greenland during the last glacial. *Nature,* **394,** 739–743.

Broccoli, A., K. Dahl, and R. Stouffer, 2006: Response of the ITCZ to Northern Hemisphere cooling. *Geophys. Res. Lett.,* **33,** L01702, doi:10.1029/2005GL024546.

Cessi, P., K. Bryan, and R. Zhang, 2004: Global seiching of thermocline waters between the Atlantic and the Indian-Pacific Ocean Basins. *Geophys. Res. Lett.,* **31,** L04302, doi:10.1029/2003GL019091.

Chang, P., B. Wang, T. Li, and L. Ji, 1994: Interactions between the seasonal cycle and the southern oscillation—Frequency entrainment and chaos in a coupled ocean-atmosphere model. *Geophys. Res. Lett.,* **21,** 2817–2820.

Chiang, J., and C. Bitz, 2005: Influence of high latitude ice cover on the marine Intertropical Convergence Zone. *Climate Dyn.,* **25,** 477–496.

Clement, A. C., R. Seager, and M. A. Cane, 1999: Orbital controls on the tropical climate. *Paleoceanography,* **14,** 441–456.

Collins, M., and the CMIP Modelling Groups, 2005: El Niño- or La Niña-like climate change? *Climate Dyn.,* **24,** 89–104.

Corrège, T., T. Delcroix, J. Récy, W. Beck, G. Cabioch, and F. L. Cornec, 2000: Evidence for stronger El Niño-Southern Oscillation (ENSO) events in a mid-Holocene massive coral. *Paleoceanography,* **15,** 465–470.

Dahl, K. A., A. J. Broccoli, and R. J. Stouffer, 2005: Assessing the role of North Atlantic freshwater forcing in millennial scale climate variability: A tropical Atlantic perspective. *Climate Dyn.,* **24,** 325–346.

Delworth, T., and M. Mann, 2000: Observed and simulated multidecadal variability in the northern hemisphere. *Climate Dyn.,* **16,** 661–676.

——, S. Manabe, and R. Stouffer, 1993: Interdecadal variations of the thermohaline circulation in a coupled ocean–atmosphere model. *J. Climate,* **6,** 1900–1989.

——, and Coauthors, 2006: GFDL's CM2 global coupled climate models. Part I: Formulation and simulation characteristics. *J. Climate,* **19,** 643–674.

Dixon, K., T. Delworth, M. Spelman, and R. Stouffer, 1999: The influence of transient surface fluxes on North Atlantic overturning in a coupled climate change experiment. *Geophys. Res. Lett.,* **26,** 2749–2752.

Dong, B., and R. Sutton, 2002: Adjustment of the coupled ocean–atmosphere system to a sudden change in the Thermohaline Circulation. *Geophys. Res. Lett.,* **29,** 1728, doi:10.1029/2002GL015229.

——, R. Sutton, and A. Scaife, 2006: Multidecadal modulation of El Niño–Southern Oscillation (ENSO) variance by Atlantic Ocean sea surface temperatures. *Geophys. Res. Lett.,* **33,** L08705, doi:10.1029/2006GL025766.

Ducet, N., P. L. Traon, and G. Reverdin, 2000: Global high resolution mapping of ocean circulation from TOPEX/Poseidon and ERS-1/2. *J. Geophys. Res.,* **105,** 19 477–19 498.

Eisenman, I., L. Yu, and E. Tziperman, 2005: Westerly wind bursts: ENSO's tail rather than the dog. *J. Climate,* **18,** 5224–5238.

Fedorov, A. V., and S. Philander, 2000: Is El Niño changing? *Science,* **288,** 1997–2002.

Galanti, E., E. Tziperman, M. Harrison, A. Rosati, R. Giering, and Z. Sirkes, 2002: The equatorial thermocline outcropping: A seasonal control on the tropical Pacific ocean–atmosphere instability strength. *J. Climate,* **15,** 2721–2739.

Gill, A., 1980: Some simple solutions for heat induced tropical circulation. *Quart. J. Roy. Meteor. Soc.,* **106,** 447–462.

Gnanadesikan, A., and Coauthors, 2006: GFDL's CM2 Global Coupled Climate Models. Part II: The baseline ocean simulation. *J. Climate,* **19,** 675–697.

Goodman, P. J., 2001: Thermohaline adjustment and advection in an OGCM. *J. Phys. Oceanogr.,* **31,** 1477–1497.

Gordon, C., C. Cooper, C. Senior, H. Banks, J. Gregory, T. Johns, J. Mitchell, and R. Wood, 2000: The simulation of SST, sea ice extents and ocean heat transports in a version of the Hadley Centre coupled model without flux adjustments. *Climate Dyn.,* **16,** 147–168.

Gregory, J., and Coauthors, 2005: A model intercomparison of changes in the Atlantic thermohaline circulation in response to increasing CO_2 concentration. *Geophys. Res. Lett.,* **32,** L12703, doi:10.1029/2005GL023209.

Griffies, S., and K. Bryan, 1997: A predictability of simulated North Atlantic multidecadal variability. *Climate Dyn.,* **13,** 459–487.

——, and Coauthors, 2006: Formulation of an ocean model for global climate simulation. *Ocean Sci.,* **1,** 45–79.

Grötzner, A., M. Latif, A. Timmermann, and R. Voss, 1999: Interannual to decadal predictability in a coupled ocean–atmosphere general circulation model. *J. Climate,* **12,** 2607–2624.

Gu, D., and S. Philander, 1995: Secular changes of annual and interannual variability in the Tropics during the past century. *J. Climate,* **8,** 864–876.

Guilyardi, E., 2005: El Niño–mean state–seasonal cycle interactions in a multi-model ensemble. *Climate Dyn.,* **26,** 329–348.

Hemming, S., 2004: Heinrich events: Massive late Pleistocene detritus layers of the North Atlantic and their global climate imprint. *Rev. Geophys.,* **42,** RG1005, doi:10.1029/2003RG000128.

Hsieh, W., and K. Bryan, 1996: Redistribution of sea level rise associated with enhanced greenhouse warming: A simple model study. *Climate Dyn.,* **12,** 535–544.

Huang, R., M. Cane, N. Naik, and P. Goodman, 2000: Global adjustment of the thermocline in response to deepwater formation. *Geophys. Res. Lett.,* **27,** 759–762.

Huygens, C., 1669: Instructions concerning the use of pendulum-watches, for finding the Longitude at Sea. *Philos. Trans. Roy. Soc.,* **4,** 937.

Ivanochko, T., R. Ganeshram, G.-J. Brummer, G. Ganssen, S. Jung, S. Moreton, and D. Kroon, 2005: Variations in tropical convection as an amplifier of global climate change at the millennial scale. *Earth Planet. Sci. Lett.,* **235,** 302–314.

Jin, F.-F., L. Lin, A. Timmermann, and J. Zhao, 2007: Ensemble-mean dynamics of the ENSO recharge oscillator under state-dependent stochastic forcing. *Geophys. Res. Lett.,* **34,** L03807, doi:10.1029/2006GL027372.

Johnson, H., and D. Marshall, 2004: Global teleconnections of meridional overturning circulation anomalies. *J. Phys. Oceanogr.,* **34,** 1702–1722.

Jungclaus, J., and Coauthors, 2006: Ocean circulation and tropical

variability in the coupled model ECHAM5/MPI-OM. *J. Climate,* **19,** 3952–3972.

Kalnay, E., and Coauthors, 1996: The NCEP/NCAR 40-Year Reanalysis Project. *Bull. Amer. Meteor. Soc.,* **77,** 437–471.

Kerr, R., 2000: A North Atlantic climate pacemaker for the centuries. *Science,* **288,** 1984–1985.

Kiehl, J., and P. Gent, 2004: The Community Climate System Model, version two. *J. Climate,* **17,** 3666–3682.

Knutson, T., S. Manabe, and D.-F. Gu, 1997: Simulated ENSO in a global coupled ocean–atmosphere model: Multidecadal amplitude modulation and CO_2 sensitivity. *J. Climate,* **10,** 138–161.

Knutti, R., J. Flückiger, T. Stocker, and A. Timmermann, 2004: Strong hemispheric coupling of glacial climate through freshwater discharge and ocean circulation. *Nature,* **430,** 851–856.

Koutavas, A., and J. Lynch-Stieglitz, 2004: Variability of the marine ITCZ over the easten Pacific during the past 30,000 years. *The Hadley Circulation: Present, Past and Future,* Springer, 347–369.

Kraus, E., and J. Turner, 1967: A one dimensional model of the seasonal thermocline. Part II. *Tellus,* **19,** 98–105.

Latif, M., M. Collins, H. Pohlmann, and N. Keenlyside, 2006: A review of predictability studies of Atlantic sector climate on decadal time scales. *J. Climate,* **19,** 5971–5987.

Lea, D., D. Pak, L. Peterson, and K. Hughen, 2003: Synchroneity of tropical and high-latitude Atlantic temperatures over the last glacial termination. *Science,* **301,** 1361–1364.

Levitus, S., 1994: World Ocean Atlas. Informal Rep. 13, National Oceanography Data Center, CD-ROM Data set Documentation, 30 pp.

Li, T., and S. G. H. Philander, 1996: On the annual cycle of the equatorial eastern Pacific. *J. Climate,* **9,** 2986–2998.

Liu, Z., 2002: A simple model study of the forced response of ENSO to an external periodic forcing. *J. Climate,* **15,** 1088–1098.

Manabe, S., and R. Stouffer, 1988: Two stable equilibria of a coupled ocean–atmosphere model. *J. Climate,* **1,** 841–866.

Marsland, S., H. Haak, J. Jungclaus, M. Latif, and F. Röske, 2003: The Max-Planck-Institute global ocean/sea ice model with orthogonal curvilinear coordinates. *Ocean Modell.,* **5,** 91–127.

Meehl, G., C. Covey, B. McAvaney, M. Latif, and R. Stouffer, 2005: Overview of the Coupled Model Intercomparison Project. *Bull. Amer. Meteor. Soc.,* **86,** 89–93.

Merryfield, W., 2006: Changes to ENSO under CO_2 doubling in a multimodel ensemble. *J. Climate,* **19,** 4009–4027.

Pacanowski, R., and S. Philander, 1981: Parameterization of vertical mixing in numerical models of tropical oceans. *J. Phys. Oceanogr.,* **11,** 1443–1451.

Peterson, L., G. Haug, K. Hughen, and U. Rohl, 2000: Rapid changes in the hydrologic cycle of the tropical Atlantic during the last glacial. *Science,* **290,** 1947–1951.

Philander, S., D. Gu, D. Halpern, G. Lambert, N.-C. Lau, T. Li, and R. Pacanowski, 1996: Why the ITCZ is mostly north of the equator. *J. Climate,* **9,** 2958–2972.

Philip, S., and G. van Oldenborgh, 2006: Shifts in ENSO coupling processes under global warming. *Geophys. Res. Lett.,* **33,** L11704, doi:10.1029/2006GL026196.

Pikovsky, A., M. Rosenblum, and J. Kurths, 2000: Phase synchronization in regular and chaotic systems. *Int. J. Bifur. Chaos,* **10,** 2291–2306.

Rayner, N., D. Parker, E. Horton, C. Folland, L. Alexander, D. Rowell, E. Kent, and A. Kaplan, 2003: Global analyses of sea surface temperature, sea ice, and night marine air temperature since the late nineteenth century. *J. Geophys. Res.,* **108,** 4407, doi:10.1029/2002JD002670.

Rein, B., A. Lückge, L. Reinhardt, F. Sirocko, A. Wolf, and W.-C. Dullo, 2005: El Niño variability off Peru during the last 20, 000 years. *Paleoceanography,* **20,** PA4003, doi:10.1029/2004PA001099.

Reynolds, R., N. Rayner, T. Smoth, D. Stokes, and W. Wang, 2002: An improved in situ and satellite SST analysis for climate. *J. Climate,* **15,** 1609–1625.

Roeckner, E., and Coauthors, 2003: The atmospheric general circulation model ECHAM5, part I: Model description. Tech. Rep. 349, Max-Planck-Institut für Meteorologie, 127 pp.

Schmittner, A., M. Latif, and B. Schneider, 2005: Model projections of the North Atlantic thermohaline circulation for the 21st century assessed by observations. *Geophys. Res. Lett.,* **32,** L23710, doi:10.1029/2005GL024368.

Seo, H., M. Jochum, R. Murtugudde, and A. Miller, 2006: Effect of ocean mesoscale variability on the mean state of tropical Atlantic climate. *Geophys. Res. Lett.,* **33,** L09606, doi:10.1029/2005GL025651.

Stocker, T. F., and S. Johnsen, 2003: A minimum thermodynamic model for the bipolar seesaw. *Paleoceanography,* **18,** 1087, doi:10.1029/2003PA000920.

Stott, L., C. Poulsen, S. Lund, and R. Thunell, 2002: Super ENSO and global climate oscillations at millenial time scales. *Science,* **297,** 222–226.

Stouffer, R., and Coauthors, 2006: Investigating the causes of the response of the thermohaline circulation to past and future climate changes. *J. Climate,* **19,** 1365–1387.

Timmermann, A., 2003: Decadal ENSO amplitude modulations: A nonlinear mechanism. *Global Planet. Change,* **37,** 135–156.

——, and F.-F. Jin, 2006: Predictability of coupled processes. *Predictability of Weather and Climate,* Cambridge University Press, 251–274.

——, M. Latif, R. Voss, and A. Grötzner, 1998: Northern Hemispheric interdecadal variability: A coupled air–sea mode. *J. Climate,* **11,** 1906–1931.

——, ——, A. Bacher, J. Oberhuber, and E. Roeckner, 1999a: Increased El Niño frequency in a climate model forced by future greenhouse warming. *Nature,* **398,** 694–696.

——, ——, and R. Voss, 1999b: Modes of climate variability as simulated by the coupled atmosphere-ocean model ECHAM3/LSG. Part I: ENSO-like climate variability and its low-frequency modulation. *Climate Dyn.,* **15,** 605–618.

——, S. An, U. Krebs, and H. Goosse, 2005a: ENSO suppression due to a weakening of the North Atlantic thermohaline circulation. *J. Climate,* **18,** 3122–3139.

——, U. Krebs, F. Justino, H. Goosse, and T. Ivanochko, 2005b: Mechanisms for millennial-scale global synchronization during the last glacial period. *Paleoceanography,* **20,** PA4008, doi:10.1029/2004PA001090.

——, S. Lorenz, S.-I. An, A. Clement, and S.-P. Xie, 2007: The effect of orbital forcing on the mean climate and variability of the tropical Pacific. *J. Climate,* **20,** 4147–4159.

Tudhope, A., and Coauthors, 2001: Variability in the El Niño–Southern Oscillation through a glacial-interglacial cycle. *Science,* **291,** 1511–1517.

Tziperman, E., L. Stone, M. Cane, and H. Jarosh, 1994: El Niño chaos: Overlapping of resonances between the seasonal cycle and the Pacific Ocean-Atmosphere Oscillator. *Science,* **264,** 72.

——, S. Zebiak, and M. Cane, 1997: Mechanisms of seasonal–ENSO interaction. *J. Atmos. Sci.,* **54,** 61–71.

Vellinga, M., R. Wood, and J. M. Gregory, 2002: Processes governing the recovery of a perturbed thermohaline circulation in HadCM3. *J. Climate,* **15,** 764–779.

Wang, B., R. Wu, and R. Lukas, 2000: Annual adjustment of the thermocline in the tropical Pacific Ocean. *J. Climate,* **13,** 596–616.

Wang, Y., S.-P. Xie, H. Xu, and B. Wang, 1999: Regional model simulations of marine boundary layer clouds over the southeast Pacific off South America. Part I: Control experiment. *Mon. Wea. Rev.,* **127,** 274–296.

Wittenberg, A., A. Rosati, N.-C. Lau, and J. J. Ploshay, 2006: GFDL's CM2 global coupled climate models. Part III: Tropical Pacific climate and ENSO. *J. Climate,* **19,** 698–722.

Wright, D., 1997: A new eddy mixing parametrization and ocean general circulation model. *International WOCE Newsletter,* No. 26, WOCE International Project Office, Southampton, United Kingdom, 27–29.

Wu, L., F. He, and Z. Liu, 2005: Coupled ocean-atmosphere response to north tropical Atlantic SST: Tropical Atlantic dipole and ENSO. *Geophys. Res. Lett.,* **32,** L21712, doi:10.1029/2005GL024222.

Xie, S.-P., 1994: On the genesis of the equatorial annual cycle. *J. Climate,* **7,** 2008–2013.

——, 1996: Effects of seasonal forcing on latitudinal asymmetry of the ITCZ. *J. Climate,* **9,** 2945–2950.

——, and Coauthors, 2007: A regional ocean–atmophere model for eastern Pacific climate: Toward reducing tropical biases. *J. Climate,* **20,** 1504–1522.

Yeager, S., C. Shields, W. Large, and J. Hack, 2006: The low-resolution CCSM3. *J. Climate,* **19,** 2545–2566.

Yu, J.-Y., and C. Mechoso, 1999: Links between annual variations of Peruvian stratocumulus clouds and of SST in the eastern equatorial Pacific. *J. Climate,* **12,** 3305–3318.

Zebiak, S. E., and M. A. Cane, 1987: A model El Niño–Southern Oscillation. *Mon. Wea. Rev.,* **115,** 2262–2278.

Zhang, R., and T. Delworth, 2005: Simulated tropical response to a substantial weakening of the Atlantic thermohaline circulation. *J. Climate,* **18,** 1853–1860.